DOI: 10.5327/Z2317-4889201400010012

INVITED REVIEW

The hot back-arc zone of the Araçuaí orogen, Eastern Brazil: from sedimentation to granite generation

A zona quente do retroarco do Orógeno Araçuaí, Brasil Oriental: da sedimentação à geração de granitos

Camila Gradim[1]*, Jorge Roncato[1], Antônio Carlos Pedrosa-Soares[1#], Umberto Cordani[2#], Ivo Dussin[1#], Fernando Flecha Alkmim[3#], Gláucia Queiroga[3], Tânia Jacobsohn[2], Luiz Carlos da Silva[4#], Marly Babinski[2#]

ABSTRACT: This article presents new lithochemical and geochronological data obtained from gneisses and granites occurring in the region located to the east of the Rio Doce calc-alkaline arc (630 – 580 Ma), which corresponds to the back-arc basin of the Araçuaí orogen. The Nova Venécia Complex, represents the most fertile source of peraluminous granitic melts in the studied back-arc zone. It mostly consists of migmatitic Al-rich paragneisses, ranging from biotite-rich gneisses to biotite-free cordierite-rich granulites, whose main protoliths were graywacky sediments. An EW-oriented section across the northern back-arc region reveals a zone rich in cordierite granulites of the Nova Venécia Complex at the base, followed by migmatites that gradually pass to the Ataléia foliated granites rich in metasedimentary enclaves, which in turn lay beneath the Carlos Chagas batholith. To the south of the Carlos Chagas batholith, orthopyroxene-bearing rocks often occur in both the Nova Venécia Complex and the Ataléia Suite, suggesting a deeper crustal level. Our U-Pb data suggest that melting processes started on the Nova Venécia Complex during the late development of the Rio Doce arc, around 590 Ma, forming autochthonous peraluminous melts related to the Ataléia Suite. Progressive anatexis and melt accumulation attained the climax around 575 Ma, leading to the development of the syn-collisional Carlos Chagas batholith. Around 545 – 530 Ma, a late to post-collisional anatectic episode formed garnet-cordierite leucogranites, mostly from the re-melting of the Ataléia and Carlos Chagas granites. A remarkable post-collisional plutonism caused widesperead re-heating of the back-arc domain from ca. 520 Ma to 480 Ma. This long lasting history (ca. 110 Ma) of granite generation in the back-arc zone requires distinct heat sources, such as asthenosphere ascent under the back-arc region in the pre-collisional stage, thrust stacking of the hot arc onto the back-arc, radiogenic heat release from the collisional thickened crust and, finally, asthenosphere uprising during the gravitational collapse of the Araçuaí orogen.

KEYWORDS: back-arc; orogenic heat; Rio Doce arc; Araçuaí Orogen; Brasiliano Event.

RESUMO: *Este artigo apresenta novos dados litoquímicos e geocronológicos obtidos de rochas gnáissicas e graníticas da zona de retroarco situada imediatamente a leste do Arco Rio Doce (630 – 580 Ma), no orógeno Araçuaí. O Complexo Nova Venécia é a mais importante fonte de fusões graníticas peraluminosas na região. Este complexo consiste, essencialmente, de paragnaisses peraluminosos migmatíticos que variam entre gnaisses ricos em biotita e cordierita-granulitos livres de biotita, cujos protolitos foram sedimentos grauvaquianos. Uma seção E-W no setor norte do retroarco revela uma zona rica em cordierita-granulito, na base, seguida por paragnaisses migmatíticos do Complexo Nova Venécia que passam, gradativamente, a granitos foliados ricos em enclaves de rochas metassedimentares (Suíte Ataléia), os quais estão sobrepostos pelo Batólito Carlos Chagas. Ao sul deste batólito, rochas a hercinita e ortopiroxênio são freqüentes no Complexo Nova Venécia e Suíte Ataléia, indicando nível crustal mais profundo. Nossos dados U-Pb evidenciam que processos anatéticos tiveram início no Complexo Nova Venécia ainda durante o desenvolvimento do Arco Rio Doce, em torno de 590 Ma, originando fusões graníticas relacionadas à Suíte Ataléia. A progressiva produção de magma granítico e sua acumulação atingiram o clímax no intervalo 575 Ma, em pleno estágio sincolisional, resultando na edificação do Batólito Carlos Chagas. Em torno de 545 – 530 Ma, adveio novo processo anatético, que originou granada-cordierita leucogranitos a partir da fusão parcial de granitos da Suíte Ataléia e Batólito Carlos Chagas. Finalmente, um marcante plutonismo pós-colisional (520–480 Ma) do tipo I causou importante re-aquecimento regional. Esta longa história (ca. 110 Ma) de produção de magmas graníticos na zona de retroarco requer diferentes fontes de calor, tais como ascenção astenosférica sob a região de retroarco durante o estágio pré-colisional, cavalgamento da base quente do arco sobre o retroarco, liberação de calor radiogênico da pilha crustal espessada no estágio colisional e, finalmente, ascenção astenosférica durante o colapso gravitacional do Orógeno Araçuaí.*

PALAVRAS-CHAVE: *retroarco; calor orogênico; Arco Rio Doce; Orógeno Araçuaí; Evento Brasiliano.*

[1]Pós-graduação em Geologia, Centro de Pesquisas Professor Manoel Teixeira da Costa, Instituto de Geociências, Universidade Federal de Minas Gerais - UFMG, Belo Horizonte (MG), Brazil. *E-mail: gradim_camila@yahoo.com.br; roncatojr@yahoo.com.br; pedrosa@pq.cnpq.br; ivodusin@yahoo.com.br*

[2]Instituto de Geociências, Universidade de São Paulo - USP, São Paulo (SP), Brazil. *E-mail: ucordani@usp.br, babinsky@usp.br*

[3]Departamento de Geologia, Universidade Federal de Ouro Preto - UFOP, Ouro Preto (MG), Brazil. *E-mail: ffalkmim@gmail.com, glauciaqueiroga@yahoo.com.br*

[4]Serviço Geológico do Brasil - CPRM, Belo Horizonte (MG), Brazil. *E-mail: luizcarlos2@gmail.com*

*Corresponding author

#Research Fellow of the Brazilian Scientific Council (CNPq).

Manuscrito ID 30087. **Recebido em:** 14/02/2014. **Aprovado em:** 17/02/2014

INTRODUCTION

The Araçuaí orogen and its counterpart located in Africa, the West Congo belt, make up an orogenic edifice edged by the São Francisco-Congo craton (Fig. 1). This confined orogenic system developed inside an end-branch (a gulf) of the Adamastor Ocean, shaped into the São Francisco-Congo paleocontinent in Neoproterozoic time (Pedrosa-Soares *et al.* 2001, 2008, 2011; Cordani *et al.* 2003; Alkmim *et al.* 2006).

Despite this singular geotectonic scenario, the Araçuaí orogen includes a few Cryogenian-Ediacaran ophiolite slivers (Pedrosa-Soares *et al.* 1998, 2001; Queiroga *et al.* 2007;Peixoto *et al.* 2013) and a well developed Ediacaran calc-alkaline arc, the Rio Doce arc (Figueiredo and Campos-Neto 1993; Nalini *et al.* 2000a; Pedrosa-Soares *et al.* 2001, 2011; Novo 2013). To the east of the Rio Doce arc (Fig. 1), the back-arc basin is now represented by high grade metasedimentary rocks (Noce *et al.* 2004; Pedrosa-Soares *et al.* 2006a; Roncato 2009; Gradim 2013).

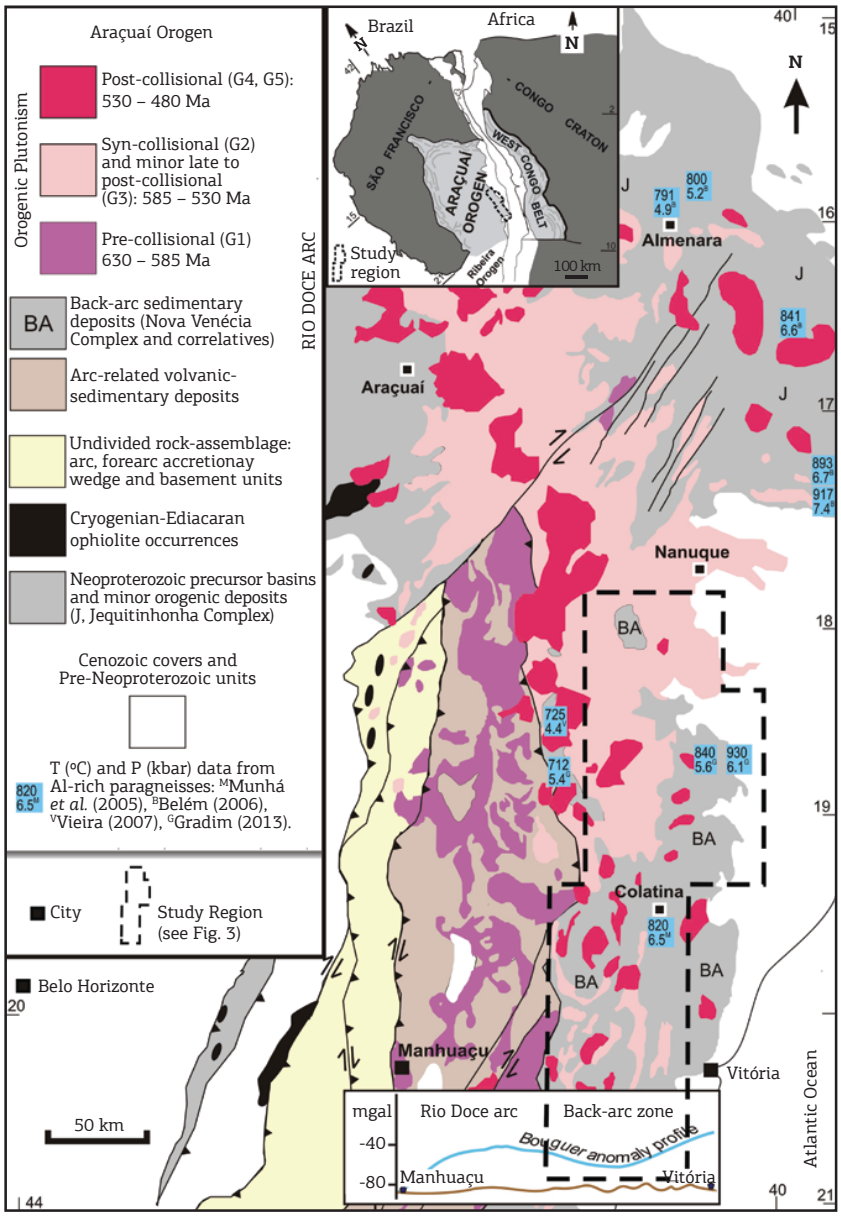

Figure 1. Geological map highlighting the main components of the Araçuaí orogen, and its paleotectonic setting (modified from Pedrosa-Soares *et al.* 2011).

The latest geological mapping projects on the focused back-arc zone were carried out by our team (Gradim *et al.* 2005; Castañeda *et al.* 2006; Queiroga *et al.* 2012; Roncato *et al.* 2012). Our maps, together with a carefully field-checked compilation of the previous maps published by Féboli (1993a,b), Signorelli (1993), Silva (1993), Vieira (1993), Tuller (1993), Baltazar (2009), and Baltazar and Silva (2009) resulted in the regional map of the studied back-arc zone (Fig. 2).

This solid field basis allowed us to select the appropriate samples from the regional rock units for petrographic, lithochemical and geochronological studies presented here. The analytical datasets can be found in Gradim (2013). Our new data allow us: (i) to determine the protoliths of the Nova Venécia gneisses, which represent the main back-arc basin infill; (ii) to constrain the maximum depositional age of the Nova Venécia basin; (iii) to outline the generation sequence and emplacement timing of the most important igneous suites in the back-arc zone; and (iv) to suggest a geotectonic model linking heat sources, magma production and the evolution of the Araçuaí orogen back-arc region.

GEOLOGICAL SETTING

From the earliest magmatic activities in the Rio Doce arc to the emplacement of the latest post-collisional intrusions, the Araçuaí orogen records a long lasting (ca. 630 – 480 Ma) succession of granite production events (Pedrosa-Soares *et al.* 2011). Regionally, these plutonic rocks have been grouped into five supersuites, namely G1–G5 (Fig. 1, Tab. 1). We summarize descriptions and data on the plutonic supersuites and related gneissic complexes from Nalini *et al.* (2000a,b), Pedrosa-Soares and Wiedemann-Leonardos (2000), Pinto *et al.* (2000), Pedrosa-Soares *et al.* (2001, 2006a,b, 2011), De Campos *et al.* (2004), Noce *et al.* (2004), Mendes *et al.* (2005), Belém (2006), Castañeda *et al.* (2006), Vieira (2007), Baltazar *et al.* (2010), Paes *et al.* (2010), Gonçalves-Dias *et al.* (2011), Silva *et al.* (2011), Queiroga *et al.* (2012), Roncato *et al.* (2012), Novo (2013), Peixoto *et al.* (2013), and references therein. The G4 supersuite was not found in the study region (Tab. 1). If not otherwise specified, the name granite is used in a general sense.

The G1 supersuite represents the plutonic portion of the pre-collisional, calc-alkaline Rio Doce arc (Fig. 1, Tab. 1). Despite its volcanic arc chemical signature, the G1 rocks show hybrid isotopic attributes (negative epsilon Nd values from -5 to -13, T_{DM} model ages from 1.2 to 2.2 Ga, inherited zircons mostly from a late Rhyacian continental crust), suggesting interaction between mantle derived magmas and the Paleoproterozoic continental basement.

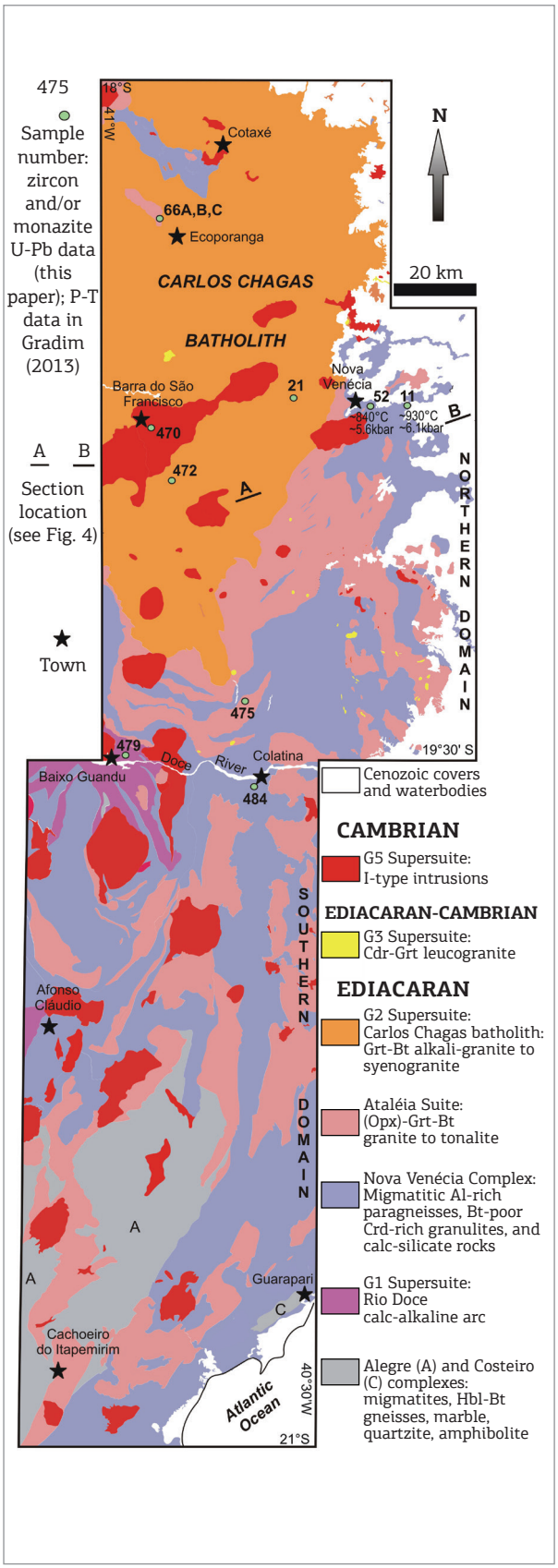

Figure 2. Geological map of the studied region (see A-B cross-section in Fig. 3).

Table 1. Main characteristics of plutonic supersuites of the Araçuaí orogen (cf. Pedrosa-Soares *et al.* 2011)

Supersuite	Lithology	Structure	U–Pb Age	Geochemical signature	Stage
G1	Mostly tonalite to granodiorite, with minor granite, generally rich in dioritic to mafic enclaves, and relatively small plutons of gabbronoritic to charnockitic composition.	Regionally foliated to banded, with locally preserved igneous features.	ca. 630 Ma to ca. 580 Ma	Metaluminous to slightly peraluminous, I-type, medium- to high-K, expanded calc-alkaline series.	Pre-collisional to early collisional
G2*	Bt+Grt±Crd±Sil±Hc±Opx syenogranite to tonalite** and Bt+Grt±Ms syenogranite to granodiorite***, generally rich in enclaves of metasedimentary rocks.	Regionally foliated to banded, with locally preserved igneous features.	ca. 590 to ca. 545 Ma	Peraluminous, mostly S-type, calc-alkaline to alkali-calcic (high-K)	Late pre-collisional to late collisional
G3	Leucogranites (Grt±Crd±Sil alkali-granite to syenogranite) rich in Bt-schlieren and enclaves from G2 granites.	Isotropic (no igneous flow, no regional foliation).	ca. 545 to ca. 530 Ma	Peraluminous, S-type, high-K alkaline	Late collisional to post-collisional
G4****	Bt+Ms±Grt granite, garnet-two-mica granite, biotite granite to granodiorite, with pegmatoid granite cupolas, rich in enclaves of metasedimentary rocks.	Isotropic to igneous flow, locally foliated along intrusive contacts.	ca. 535 to ca. 500 Ma	Peraluminous, mostly S-type, high-K alkaline	Post-collisional
G5	Mostly Bt±Hbl±Opx syenogranite to granodiorite (including charnockitic equivalents), minor norite to enderbite.	Isotropic to igneous flow, locally foliated along intrusive contacts.	ca. 520 to ca. 480 Ma	Metaluminous to slightly peraluminous, I- and A2-types, high-K-Fe calc-alkaline to alkaline, minor tholeiitic terms.	Post-collisional

*I-type G2 granites omitted. **Predominance in the central to southern, and ***in the northern regions of the Araçuaí orogen. ****Not found in the studied back–arc zone.

Supracrustal successions related to the Rio Doce magmatic arc include the metavolcano-sedimentary formations of the Rio Doce Group and the metasedimentary rocks of the Nova Venécia Complex, representing arc covers and a back-arc basin, respectively (Figs. 1 and 2).

The collisional stage of the Araçuaí orogen was accompanied by regional deformation and metamorphism, imposing anatectic processes on gneissic complexes under amphibolite to granulite facies conditions. In the eastern Araçuaí orogen, a large amount of granitic rocks was generated from the partial melting of Al-rich paragneisses of the Nova Venécia and Jequitinhonha complexes (Fig. 1).

The G2 supersuite represents an essentially collisional granite population, mostly including peraluminous granites (Tab. 1). G2 peraluminous granites form a continuous NS-trending belt that extends for over 350 km between the towns of Colatina and Almenara (Fig. 1). This granite belt includes distinct suites, varying in composition and/or grain size. The southern part of this belt includes the Carlos Chagas batholith and Ataleia Suite (Fig. 2).

The G3 supersuite is much less voluminous and generally occurs in close spatial association with G2 granites. A typical G3 rock is a biotite-free leucogranite, generally forming leucosomes overprinting the host G2 granite (Tab. 1).

The G5 supersuite includes balloon-like zoned plutons composed of granitic and mafic rocks, characterizing a bimodal plutonic assemblage (Tab. 1). Outstanding features revealed by G5 plutons are diapir roots with inverse zoning

(mafic cores and granitic borders), as well as widespread evidence of magma mixing. G5 intrusions usually disturb the regional structural trend, shaping the regional foliation around them. Although they are free from the regional foliation, they may show a local foliation developed along their margins owing to emplacement-related stresses.

A Bouguer anomaly profile shows a gravimetric low corresponding to the focused back-arc zone (Fig. 1), in relation to the Rio Doce arc and the Atlantic margin (Haralyi and Hasui 1982; Wiedemann *et al.* 2002). Such gravimetric low suggests the preservation of a relatively thick continental crust, rich in metasedimentary rocks, which may correspond to the Nova Venécia Complex, located between the Afonso Cláudio and Guarapari towns (Fig. 2). Toward its eastern border, the Bouguer profile shows a striking rise, already within the influence of the Atlantic Ocean floor in the Vitória city region (Fig. 1), but possibly also indicating a transition to a relatively thin, high-density (granulitic) continental crust.

THE NOVA VENÉCIA COMPLEX AND ASSOCIATED PLUTONISM

We summarize the main field relations and petrographic features of the Nova Venécia Complex, Ataléia Suite, Carlos Chagas batholith, and G3 leucogranites (Fig. 2). Definitions, detailed descriptions and specific studies on these units can be found in Cordani (1973), Bayer *et al.* (1986), Silva *et al.* (1987), Sluitner and Weber-Diefenbach (1989), Pinto *et al.* (2000), Pedrosa-Soares and Wiedemann-Leonardos (2000), De Campos *et al.* (2004), Pedrosa-Soares *et al.* (2006a,b, 2011), Noce *et al.* (2004), Castañeda *et al.* (2006), Baltazar *et al.* (2010), Roncato (2009), Roncato *et al.* (2012), Queiroga *et al.* (2012), Gradim (2013) and Richter (2013). Rocks of the Nova Venécia Complex and Ataléia Suite were formerly included in the Alegre, Costeiro and Paraíba do Sul complexes, and called as "kinzigites" and "kinzigitic gneisses" in former papers. We use mineral name abbreviations recommended by Siivola and Schmid (2007).

The study region shows two tectono-metamorphic domains, roughly limited at the surface by the Doce River (Fig. 2). The northern domain, dominated by the Carlos Chagas batholith, shows a general west-dipping structure verging to the east. The regional structure of the southern domain, dipping to the east and verging to the west, is cut by important NE-SW strike-slip shear zones. In general, this domain represents a deeper crustal level, relatively richer in granulite facies rocks than the northern one. In both domains, amphibolite facies rocks prevail to the west, whereas granulite facies rocks (with orthopyroxene or not) often occur to the east, indicating the exposure of deeper crustal levels along the eastern sector.

The Nova Venécia Complex and Ataléia Suite extend from the surroundings of Nova Venécia to the regions of Afonso Cláudio and Guarapari. However, the Carlos Chagas batholith is an exclusive feature of the northern tectono-metamorphic domain (Fig. 2). Therefore, this domain shows the most complete crustal succession of the back-arc zone within the study region (Fig. 3). This section reveals a zone rich in Bt-poor Crd-rich granulites of the Nova Venécia Complex, at the base, followed by a series of migmatites that gradually pass to the Ataléia foliated granites rich in metasedimentary enclaves, laying beneath the Carlos Chagas batholith (Fig. 3).

The Nova Venécia Complex

Despite variation in the metamorphic assemblages, the Nova Venécia Complex is a quite homogeneous unit, consisting of migmatitic Al-rich paragneisses with lenses of calc-silicate rocks (Figs. 2, 4 and 5). Regionally, the migmatitic Al-rich paragneisses represent a metamorphic rock series, including

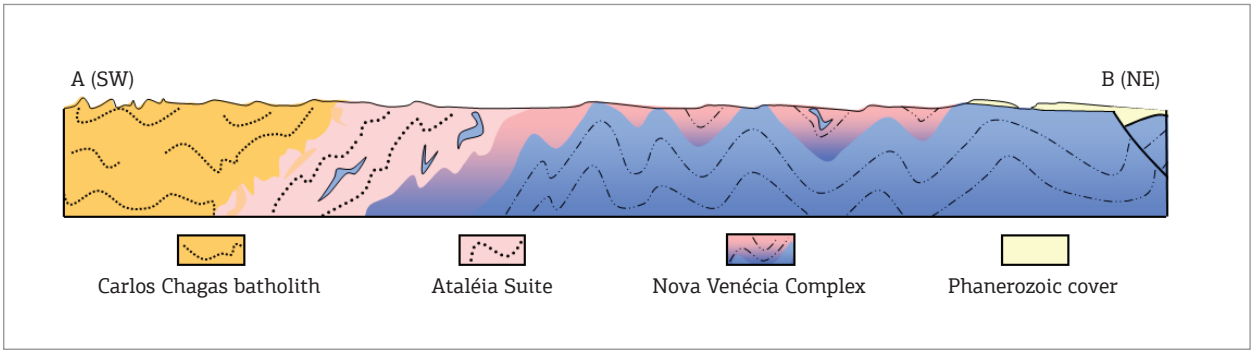

Figure 3. Cross-section showing the major relations between the Nova Venécia Complex, Ataléia Suite and Carlos Changes batholith (see location in Fig. 2).

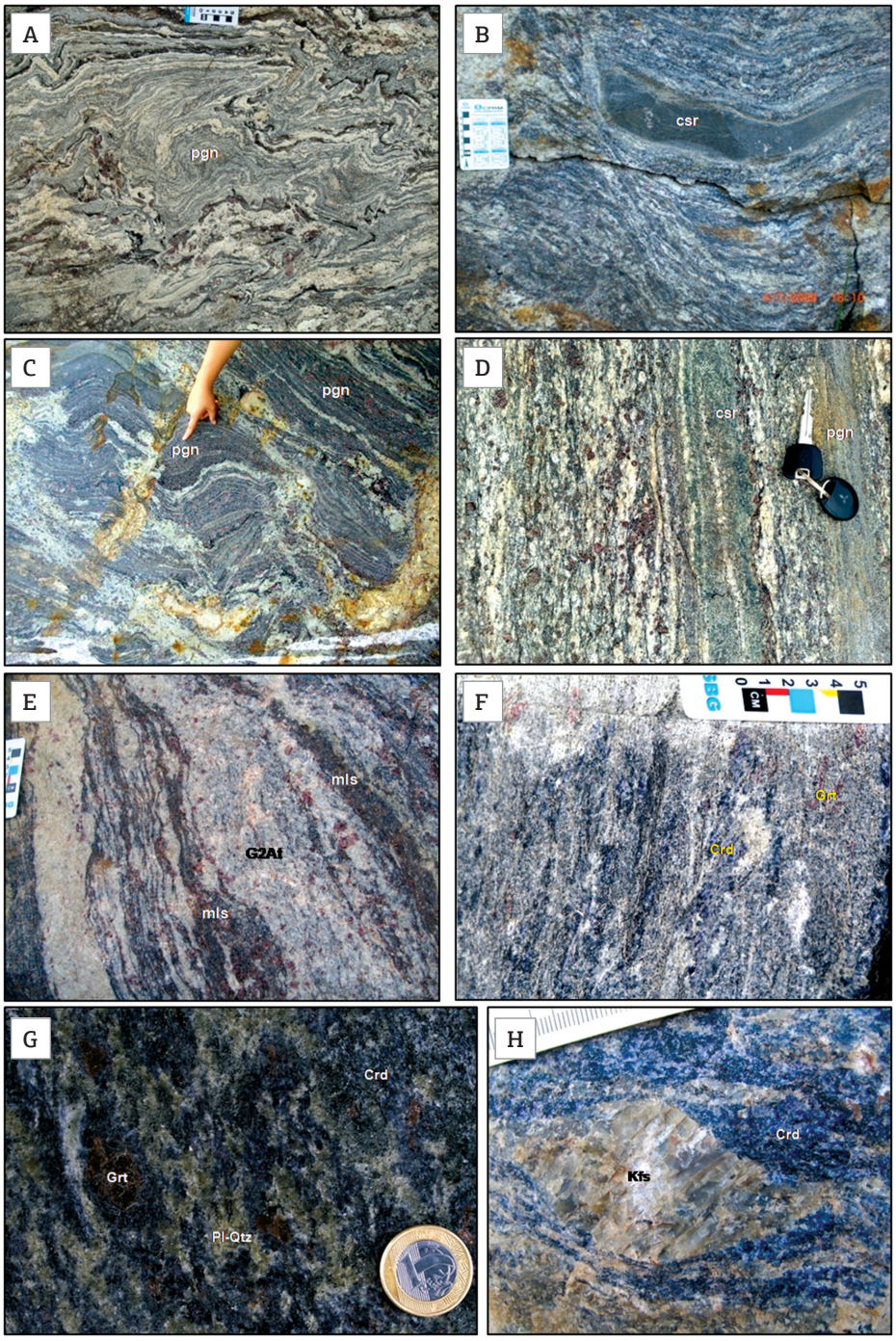

Figure 4. Photos from rocks of the Nova Venécia Complex. (A) folded stromatic migmatite showing the Grt-Bt paragneiss (pgn), and Bt-poor leucosomes (light-coloured) with associated Bt-rich melanosomes (dark gray to black); (B) calc-silicate rock (csr) enveloped by migmatitic paragneiss; (C) transitional stromatic-to-schollen migmatite; (D) diatexite showing Grt-rich leucosomes and Bt-rich melanosomes grading to paragneiss (pgn), with intercalation of calc-silicate rock (csr); (E) diatexite rich in foliated leucosomes (G2At, Ataléia-type granite) and (Opx)-Grt-Crd melanosomes relatively poor in biotite (mls), with minor Bt-bearing leucogranitic leucosomes; (F) Bt-Grt-Sil-Crd paragneiss (a Bt-bearing cordierite granulite) rich in stretched blue cordierite poikiloblasts (Crd, see Fig. 6D); (G) cordierite granulite with greenish felsic components (mostly plagioclase and quartz, Pl-Qtz) and minor garnet (Grt); (H) sigmoidal porphyroblast of K-feldspar in a blue cordierite (Crd) granulite.

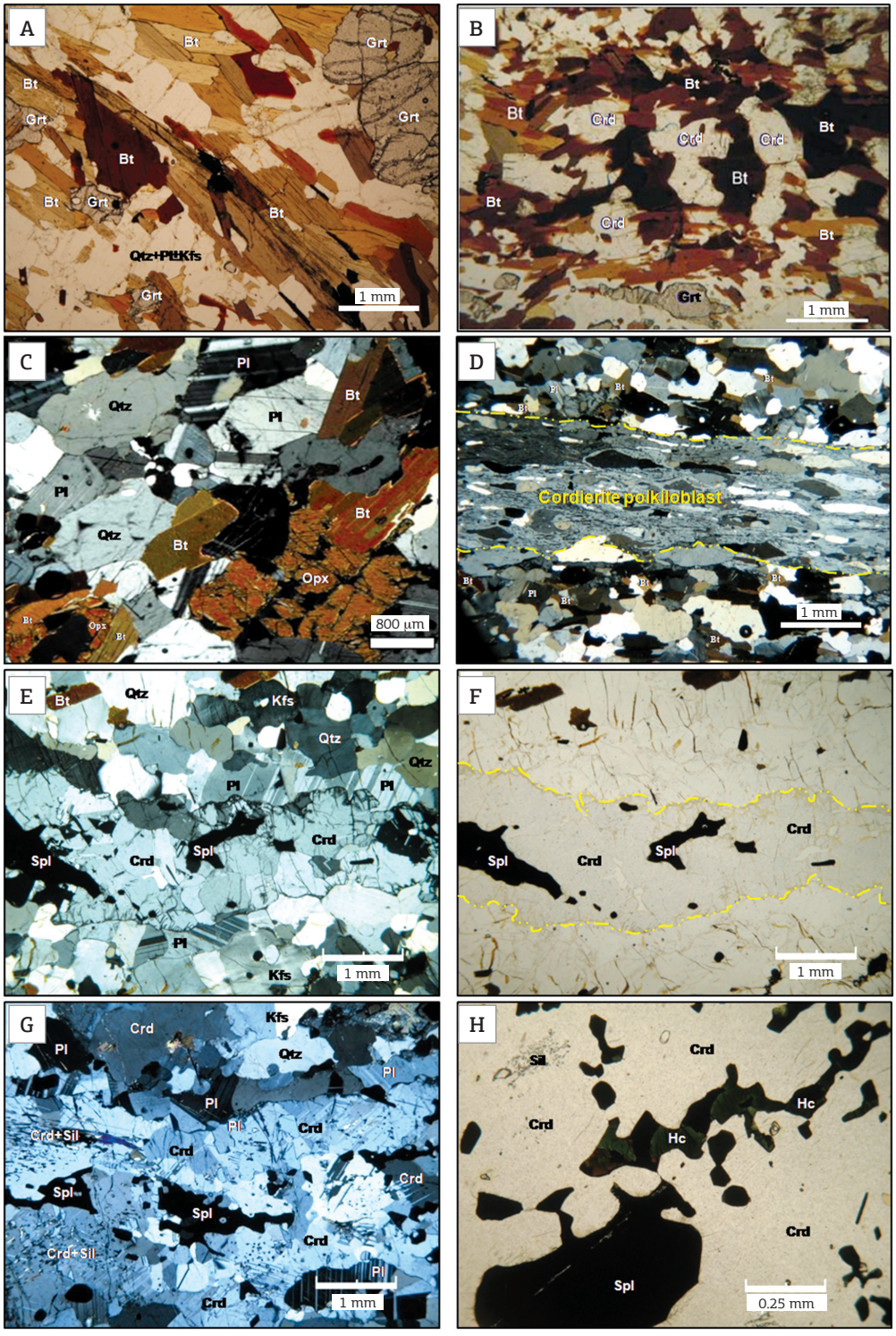

Figure 5. Photomicrographs from thin sections of rocks of the Nova Venécia Complex (A, B, F, and H, single polarizer; C, D, E and G, crossed polarizers). (A) Grt-Bt-rich paragneiss; (B) Crd-Bt-rich paragneiss; (C) Opx-bearing biotitic paragneiss; (D) stretched cordierite poikiloblast rich in quartz and sillimanite inclusions, in the Bt-bearing cordierite granulite; (E and F) Bt-poor cordierite granulite showing a stretched cordierite porphyroblast with spinel inclusions; (G) Bt-free cordierite granulite; (H) oriented spinel inclusions with green hercynite in a cordierite porphyroblast of a cordierite granulite.

amphibolite to granulite facies Sil-Crd-Grt-Bt gneisses (Figs. 4A-4D, 5A and 5B) and Bt-poor Sil-Grt-Crd granulitic gneisses (Figs. 4F to 4H and 5D to 5H), which may locally contain orthopiroxene (Fig. 5C). For descriptive purposes, we call the migmatitic Crd-Grt-Bt gneisses as paragneisses (independently of metamorphic facies), and the Bt-poor Sil-Grt-Crd gneisses as cordierite granulites or blue granulites.

The most common paleosomes of the Nova Venécia migmatites are paragneisses consisting of variable amounts of quartz, plagioclase, K-feldspar, biotite, garnet, cordierite, sillimanite and/or orthopyroxene (Figs. 5A to 5C). Accessory minerals include spinel (magnetite, hercynite), ilmenite, apatite, monazite, titanite, zircon, and sulphides. Some general features of the paragneisses are: (i) plagioclase is generally more abundant than K-feldspar in the paleosomes; (ii) biotite content decreases with the increasing amount of cordierite and/or garnet and/or leucosomes; and (iii) orthopyroxene locally occurs in both biotitic paragneisses and cordierite granulite along the eastern portion of the Nova Venécia Complex.

The laminated to banded structures of the paragneisses represent variations in mafic versus felsic mineral contents. They may be inherited from sedimentary protoliths, or formed from metamorphic banding associated with tectonic transposition. Leucosomes generally highlight the banded structures (as partial melting preferentially starts along mica-rich horizons). Paragneisses and calc-silicate rocks may show sharp contacts or gradually pass one to another (Fig. 4B), providing the best evidence of relict stratification. The calc-silicate rocks mostly consist of quartz, Ca-rich plagioclase, clinopyroxene, orthopyroxene, Ca-rich garnet, apatite, and opaque minerals.

Sil-Grt-Crd gneisses poor to free in biotite, the so-called cordierite granulites, occur in the eastern sector of the back-arc zone, and in exposures of the Nova Venécia Complex located between the towns of Ecoporanga and Cotaxé (Fig. 2). They vary in composition from Bt-Grt-bearing Crd-rich gneisses (Figs. 4F, 5D to 5F) to Bt-free Hc-Sil-Crd granulites free to poor in garnet (Figs. 4G and 4H, 5G and 5H). The Bt-poor granulites consist of quartz, plagioclase, K-feldspar, blue cordierite, garnet, sillimanite, spinel (hercynite, magnetite), orthopyroxene, apatite, and zircon (Figs. 5D to 5H). The cordierite granulites form layers and lenses grading to migmatitic paragneisses. They also form large massifs relatively poor in granitic leucossomes, which have been quarried for blue dimension stone production (Machado-Filho 1998).

Regionally, the syn-kinematic mineral assemblages related to the regional foliation are: (i) Qtz + Pl + Kfs + Bt + Grt + Crd + Sil + Ilm ± Spl ± Opx, for the migmatitic paragneisses; and (ii) Qtz + Pl + Crd + Sil + Hc + Kfs + Spl ± Grt ± Bt ± Opx, for the cordierite granulites. The Nova Venécia paragneisses are Opx-free and richer in biotite along the western sector of the back-arc zone. They tend to be Opx-bearing, and richer in cordierite, garnet and sillimanite towards the eastern border of the region. This compositional change reflects a general prograde metamorphism, varying from amphibolite facies in the west to granulite facies in the east. Available geothermobarometric data also suggest this west to east prograde metamorphism, recording temperatures from ca. 712°C in the western edge of the back-arc zone, to ca. 930°C in its eastern margin, with values around 820°C in the central part of the study region (Fig. 1; data from Munhá *et al.* 2005, and Gradim 2013). The lowest temperature (712 ± 32°C at 5.4 ± 0.5 kbar) was obtained from a Sil-Crd-Grt-Bt paleosome of a stromatic metatexite, whereas the highest temperatures were obtained from melt-poor cordierite granulites (840 ± 60°C at 5.6 ± 0.9 kbar, and 930 ± 118°C at 6.1 ± 0.4 kbar; Gradim 2013). The melt-rich Sil-Grt-Bt-Crd paragneisses from the central part of the back-arc zone yielded a temperature of 820 ± 20°C at 6.5 ± 0.5 kbar (Munhá *et al.* 2005). This increase in metamorphic temperatures agrees with the regional changes in mineral assemblages from amphibolite to granulite facies, as well as with the crustal architecture of the back-arc zone (Fig. 3). It is also in agreement with the west to east prograde metamorphism observed more to the north, in the Jequitinhonha Complex (Fig. 1), where temperatures lower than 800°C and higher than 900 °C have been determined by quantitative geothermobarometric studies (Belém 2006).

Some features provide evidence of high-grade post-kinematic reactions in the Nova Venécia gneisses, namely: (i) recrystallization of helicitic garnet overprinting the regional foliation; (ii) cordierite overgrowth on garnet forming corona textures; and (iii) development of Crd+Sil+Hc and Crd+Sil+Grt+Opx+Hc isotropic assemblages associated with the complete removal of biotite from the foliation. These features generally occur in the vicinity of G5 intrusions.

The first regional anatectic event in the Nova Venécia paragneisses gave rise to syn-deformational neossomes, whose mineral assemblages vary considerably along the study region. In the western sector of the back-arc zone, neossomes are Opx-free, and tend to be richer in biotite and relatively poor in cordierite, garnet and/or sillimanite (Fig. 4A). In the eastern sector, this syn-kinematic melting event generated usually more dehydrated neossomes, including Grt-rich leucosomes and melanosomes relatively poor in biotite, but rich in cordierite, garnet and sillimanite, locally with orthopyroxene (Fig. 4D and 4E). In fact, the migmatitic paragneisses include several metatexite and diatexite varieties (Fig. 4A to 4E), characterizing a rock assemblage formed by increasingly dehydrated anatectic products. Lenses of calc-silicate rocks represent refractory resisters in the Nova Venécia migmatites (Fig. 4B). Diatexites show granite leucosomes

similar to the Ataléia granitic rocks (Fig. 4E). These diatexites gradually pass to large bodies of Ataléia-type granites, enveloped by the migmatitic paragneisses.

The Ataléia Suite

The granitic rocks grouped in the Ataléia Suite occur in close spatial association with migmatites of the Nova Venécia Complex, as well as in large massifs (Figs. 2, 4A to 4E, 6A). Generally, the Ataléia granites are rich in paragneiss and/or calc-silicate enclaves, suggesting an essentially autochthonous nature (Figs. 6A and 6C). In fact, there is a consensus in the literature that the "kinzigitic" migmatites rich in garnet-biotite leucosomes gradually pass to larger foliated granite bodies.

Based on field and petrographic evidence, we also consider the Ataléia granites as autochthonous to semi-authochtonous melts formed from anatexis of the Nova Venécia paragneisses (Figs. 4A to 4E, 6A to 6E). Most of them clearly show the regional foliation (Figs. 6 and 7), although it may be difficult to recognize it in Bt-poor granites. Locally, they exhibit well-developed mylonitic features.

The Ataléia Suite ranges in composition from prevailing granodiorite and granite to minor tonalite. These granitic rocks include variable contents of quartz, plagioclase, K-feldspar, biotite, garnet, cordierite, sillimanite, orthopyroxene, apatite, spinel minerals (magnetite, hercynite), ilmenite, monazite, zircon, and sulphides (i.e. despite differences in mineral contents, this is the same general composition of the Nova Venécia paragneisses). Biotite and/or garnet are ubiquitous in the Ataléia granites, reaching modal values around 10 – 15%. The Pl-Grt-Opx-Hc assemblage occurs in the less evolved melts closely associated with the Nova Venécia migmatites, as well as in some large charnoenderbitic bodies (Figs. 7C and 7D). The greenish-colour, foliated, Grt-Opx-bearing granitic rocks, ranging in composition from enderbite to charnockite, are more abundant along the eastern sector of the back-arc region, mainly in the southern domain. Enclaves of calc-silicate rocks and paragneisses are very common (Fig. 6).

The regional solid-state foliation is ubiquitous and pervasive in the Ataléia granites, locally showing mylonitic features, representing the preferred orientation of biotite and/or fibrous sillimanite, as well as stretched quartz, feldspar, garnet and/or cordierite (Figs. 6 and 7).

The Carlos Chagas Batholith

The Carlos Chagas batholith extends continuously for more than 14,000 km^2 in the back-arc region of the Araçuaí orogen, approximately between latitudes 17° and 19° S (Figs. 1 and 2). It includes granites from the Carlos Chagas, Montanha and Nanuque suites, which differ from each other only in the biotite content. The batholith is thus quite homogeneous in composition, mostly consisting of leucocratic, very coarse- to medium-grained, Grt-Bt syenogranite rich in K-feldspar megacrysts (Fig. 8). Rare enclaves of Grt-Bt gneisses and calc-silicate rocks are found elsewhere in the batholith, probably representing xenoliths in distinct stages of assimilation (Fig. 8D).

Despite its homogeneous composition, the Carlos Chagas batholith is structurally heterogeneous (Fig. 8). Undeformed and deformed granites coexist within the batholith. Progressive imprint of solid-state deformation features over magmatic fabrics can be observed from outcrop to thin section scale (Figs. 8 and 9). The most commnon magmatic features displayed by the undeformed granites are: (i) isotropic structure showing chaotic euhedral K-feldspar megacrysts with well-preserved twinning boundaries and facets (Figs. 8A and 8B); (ii) igneous flow orientation of euhedral K-feldspar crystals (Figs. 8C to 8E); and (iii) isotropic structure with no evidence of intracrystalline deformation (Fig. 9A). Evidence of the syn-kinematic solid-state deformation includes the following features: (i) development of the solid-state foliation from incipient ductile deformation in the quartz-rich matrix to the remarkable development of quartz ribbons and stretched garnets (Figs. 9B, 9E and 9F); (ii) development of augen structure with K-feldspar porphyroclasts oriented according to the regional foliation (Figs. 8E to 8H); (iii) stretched quartz, K-feldspar and garnet along the regional foliation (Figs. 8F to 8K and 9D to 9F); (iv) rotated sigmoidal K-feldspar and garnet crystals showing recristallization tails (Figs. 8G to 8J); and (v) biotite breakdown and development of hercynite-sillimanite-rich trails along the regional foliation (Figs. 8K, 9C, 9D and 9G).

The structural heterogeneity of the Carlos Chagas batholith is associated with changes in the mineralogical composition, as a consequence of syn-kinematic metamorphic reactions in the deformed granites. The greater the ductile strain, the most distinctive is the accessory mineral assemblage in relation to the undeformed granites. The mineral assemblage of the undeformed granites includes quartz, perthitic K-feldspar, sodic plagioclase, biotite and garnet, with apatite, monazite, zircon, ilmenite and sulphides as accessory minerals (Fig. 9A). This mineral assemblage remained essentially stable in the less deformed granites, despite the recrystallization of biotite and quartz along the regional foliation (Fig. 9B). As the ductile deformation develops, augen structure and mylonitic features become evident (Figs. 8F to 8K). Biotite is progressively replaced, thereby generating Hc-Sil-Grt ultramylonites. (Figs. 8J and 8K, 9E and 9G). Such rocks are poor to free in biotite, recording the most dehydrated metamorphic products in the Carlos Chagas batholith. Geothermobarometric data from mylonitic Sil-Grt-Bt granites constrain the minimum metamorphic temperature for the Bt-free ultramylonites around 680°C (Pedrosa-Soares *et al.* 2011).

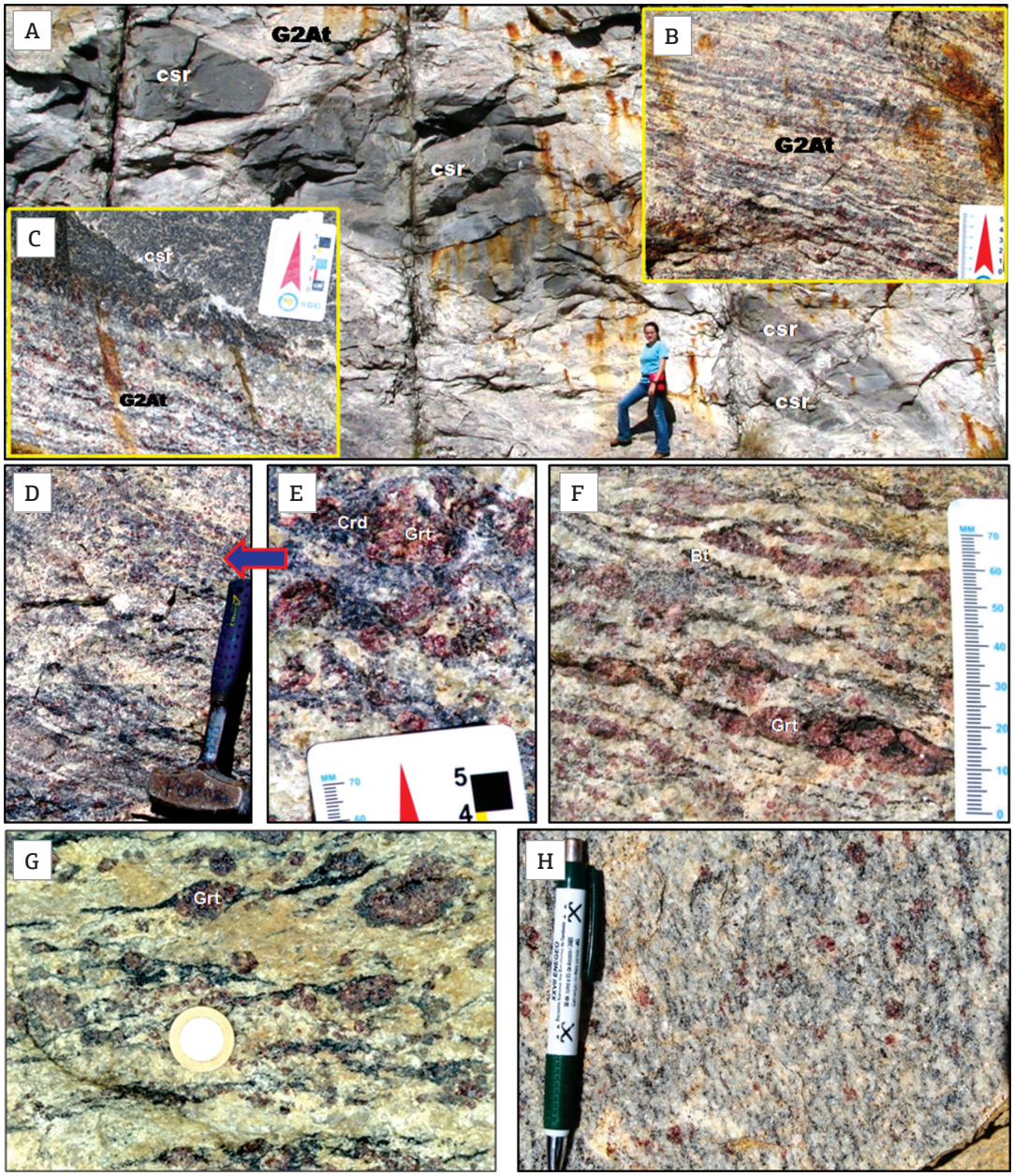

Figure 6. Photos from rocks of the Ataléia Suite. (A) large calc-silicate enclaves parallel to the regional foliation of the host Ataléia granite; (B) Bt-Grt foliated granite with melanocratic bands/laminae suggesting residual material from the partial melting process; (C) detail of the sharp contact between the calc-silicate rock and the foliated granite; (D and E) descontinous bands of Grt-Crd-rich residuum, showing cordierite overgrowths on garnets (corona texture); (F) a foliated Grt-rich granite; (G) garnet porphyroclasts with Bt-rich recrystallization tails; (H) a foliated Bt-Grt granite.

The G3 Supersuite

The G3 leucogranites form vein- to irregular-shaped leucosomes associated with G2 granites of both the Ataléia Suite and the Carlos Chagas batholith (Fig. 10A to 10C), as well as some large bodies with enclaves of G2 granites (Fig. 2). Most G3 leucogranites show gradual and irregular contacts with the parent G2 granites (Figs. 10A to 10C), suggesting autochthonous partial melting and melt crystallization processes. Rarely, sharp and interfingering contacts outline well-shaped veins and small plutons that seem to be semi-autochthonous to allochthonous. Oversized G3 leucogranite plutons reach up to 2 km in diameter, and are generally associated with the Ataléia Suite (Fig. 2).

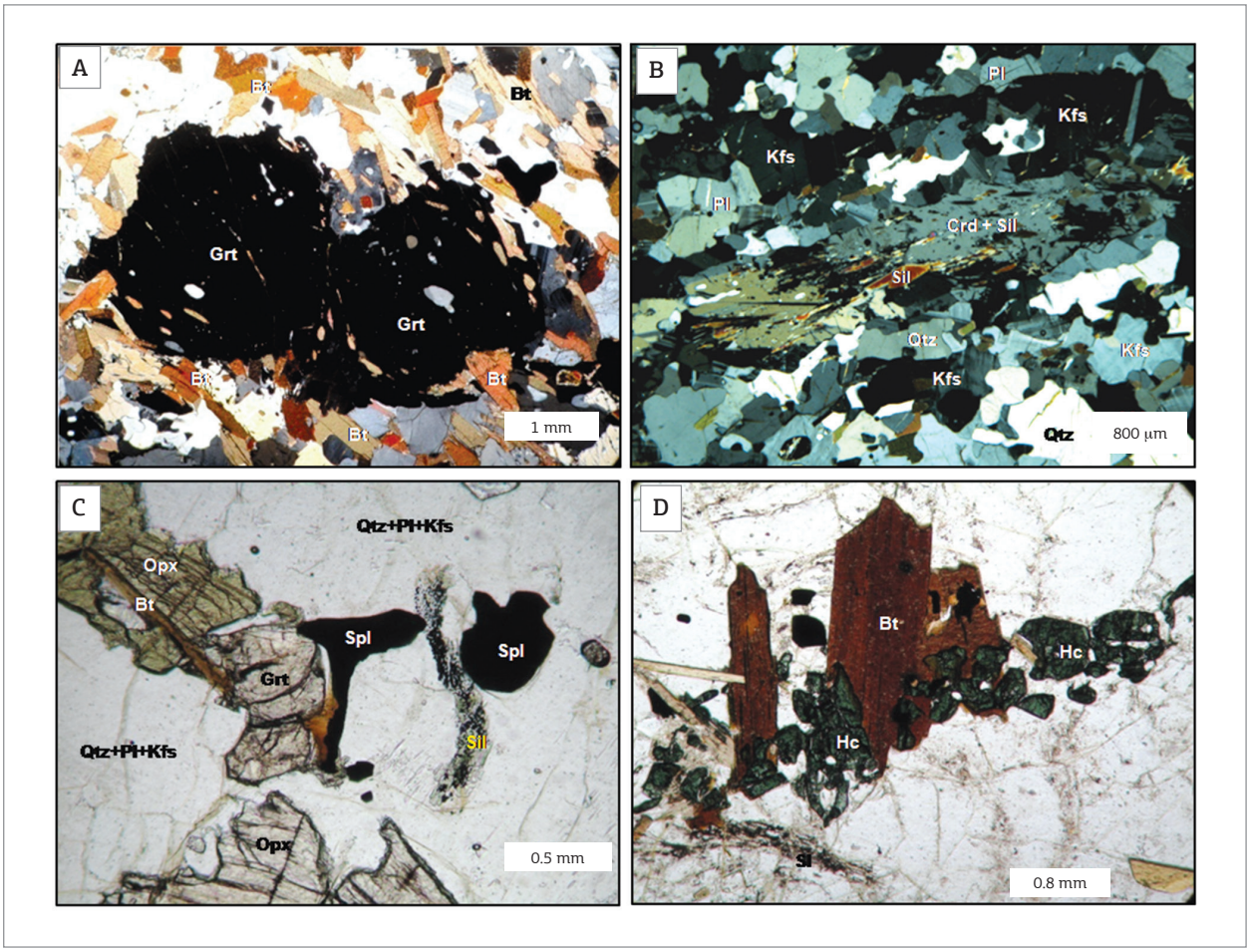

Figure 7. Photomicrographs from thin sections of rocks from the Ataléia Suite (A and B, crossed polarizers; C and D, single polarizer). (A) foliated Bt-Grt granite showing syn-kinematic, rotated inclusion trails in garnet porphyroblasts; (B) foliated Crd-Sil-Bt granite showing a stretched cordierite porphyroblast rich in oriented sillimanite inclusions parallel to the ductile foliation; (C) deformed Grt-Sil-Opx-bearing charnoenderbite; (D) green spinel (hercynite) in charnoenderbite of the Ataléia Suite.

The G3 leucogranites are rich in perthitic K-feldspar, ranging from alkali-feldspar granites to syenogranites, including sodic plagioclase (mostly in perthite), quartz, garnet and/or cordierite, sillimanite, apatite, monazite, zircon and scarce opaque minerals (Figs. 10D, 10E and 10G). They include irregular-shaped, dark-coloured, isotropic bodies consisting of cordierite, garnet, sillimanite, apatite, monazite, ilmenite and spinel (G3r in Fig. 10F). These bodies, extremely rich in peraluminous, mafic and refractory minerals, represent residual material from the partial melting process, segregated from the G3 melt (G3m in Fig.10F).

Thermal effects related to G5 plutonism

A myriad of G5 intrusions occur in the study region (Fig. 2). They range in size from large plutons to thin dykes. I-type granites and charnockites prevail in large plutons, whereas enderbites and norites are more frequent in small plutons.

The host rocks show clear changes in fabrics and mineral assemblages close to the contact with G5 intrusions. This re-heating episode caused dehydration metamorphic reactions on the Nova Venécia paragneisses, as well as on G2 and G3 granites, forming mineral assemblages rich in cordierite, garnet, sillimanite and/or spinel, and poor to free in biotite. The greenish dimension stone commercially called "Eucaliptus Green Granite", a granite rich in light-green cordierite and green spinel (hercynite) formed from the breakdown of biotite (Fig. 9H), is a product of the thermal metamorphism imposed by G5 intrusions on G2 and G3 granites.

It seems that the G5 re-heating episode reached large scale importance, promoting resetting of the mineral isotopic systems, even far from the surface traces of intrusive contacts (Cordani 1973; Munhá *et al.* 2005; Cordani *et al.* 2005).

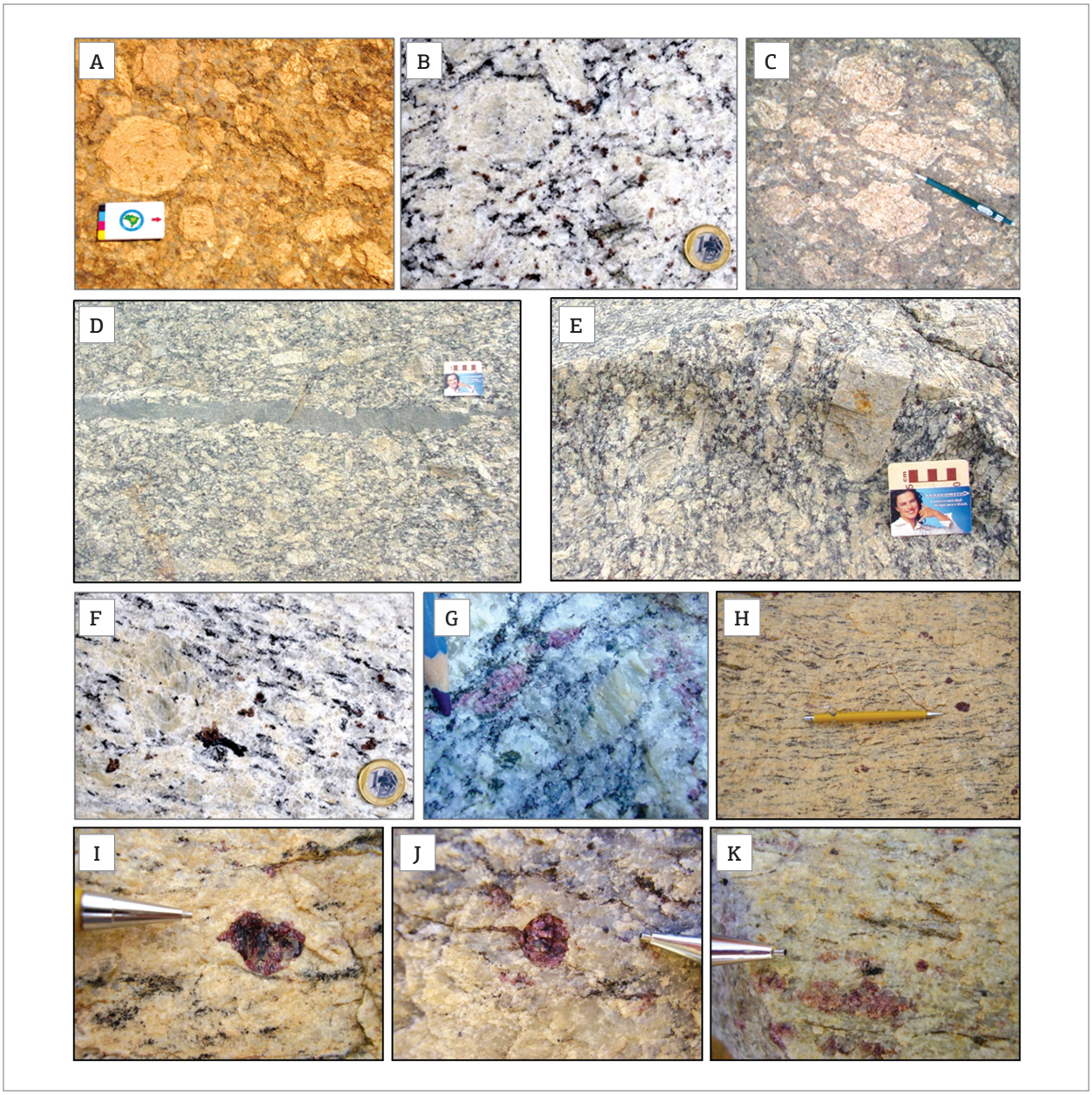

Figure 8. Photos from rocks of the Carlos Chagas batholith. (A) non-deformed isotropic Carlos Chagas granite with euhedral megacrists of K-feldspar; (B) isotropic Carlos Chagas granite in a fresh rock exposure; (C) igneous flow with euhedral K-feldspar megacrists; (D) Bt-rich enclave along the igneous flow; (E) transition from igneous flow to ductile deformation, showing euhedral as well as eye-shaped (*augen*) K-feldspar megacrysts; (F) foliated granite showing oriented biotite and eye-shaped K-feldspar crystals (*augen* structure); (G) sigmoidal K-feldspars and stretched garnets along the regional foliation; (H) mylonitic granite with stretched eye-shaped K-feldspars; (I) sigmoidal garnet; (J) rotated garnet with recrystallization tail; (K) ultramylonitic granite with stretched garnets (red) and greenish Hc-Sil-rich trails.

LITHOCHEMISTRY

We present here an evaluation of possible sedimentary protoliths of the Nova Venécia paragneisses and cordierite granulites, as well as a comparative study concerning these metasedimentary rocks and the G2 and G3 granites. Major and trace elements data from 96 rock samples, as well as sample preparation and analytical procedures are available in Gradim (2013), together with data selected from Tuller (1993) and Baltazar *et al.* (2010).

From sediments to gneisses

The main lithochemical criteria used to evaluate protoliths of carbonate-free clastic sediments are the relative distribution of the following ratios: (i) SiO_2/Al_2O_3, a maturity index for

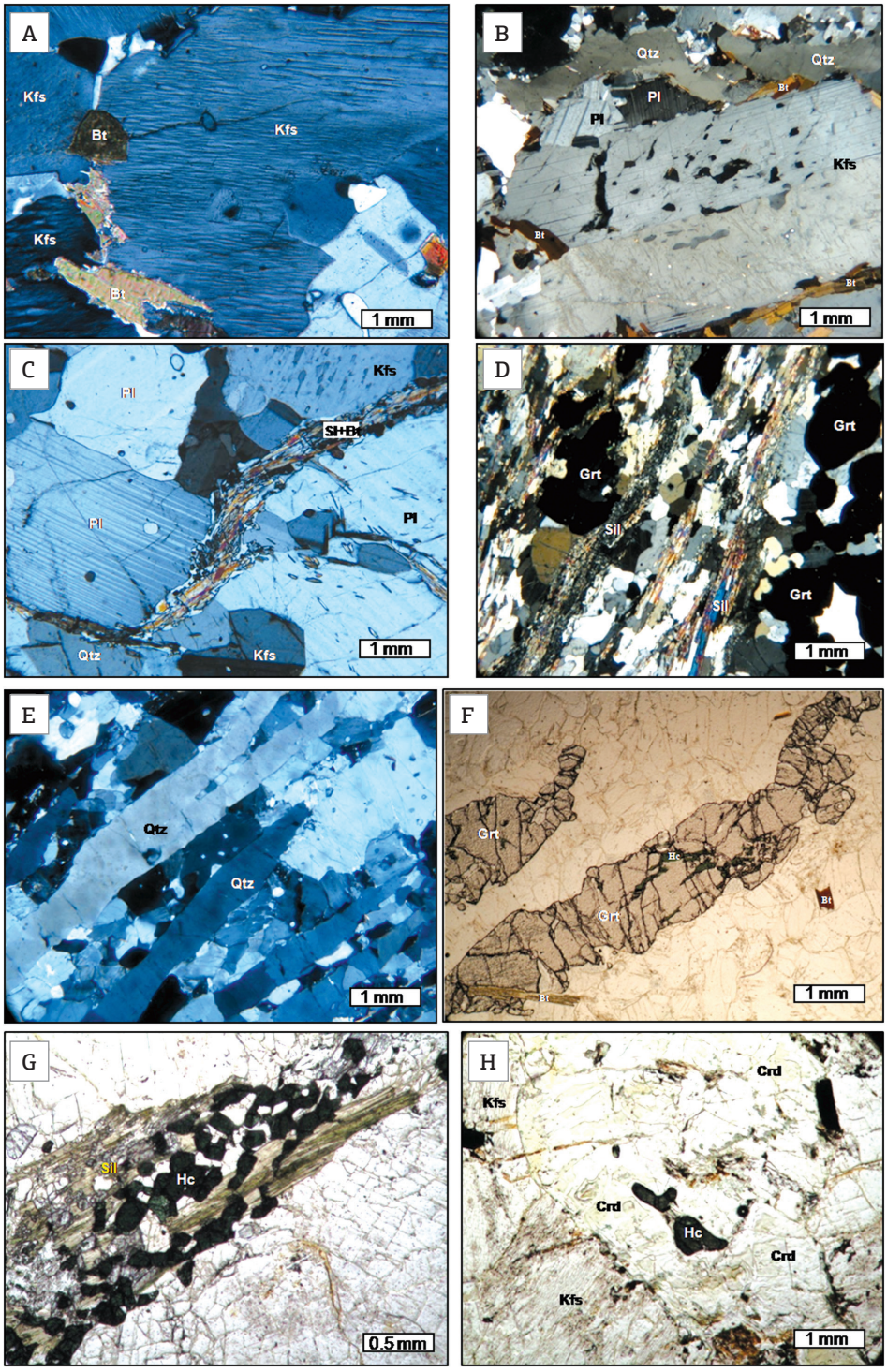

Figure 9. Photomicrographs from thin sections of rocks from the Carlos Chagas batholith (A, B, C, D and E, crossed polarizers; F, G and H, single polarizer). (A) isotropic granite rich in K-feldspar; (B) incipient ductile deformation in the Qtz-rich matrix close to an euhedral K-feldspar crystal with undeformed Carlsbad twin; (C) development of solid-state deformation marked by recrystallization of a Bt-Sil trail; (D) penetrative foliation marked by recrystallization of Sil-rich trails; (E) foliation marked by recrystallization of quartz ribbons and stretched feldspars; (F) stretched garnet crystals in mylonitic granite; (G) Bt-free Hc-Sil-rich foliation trail in ultramylonitic granite; (H) greenish cordierite and spinel (hercynite) in a non-deformed Bt-free Carlos Chagas granite (the "Eucaliptus Green Granite").

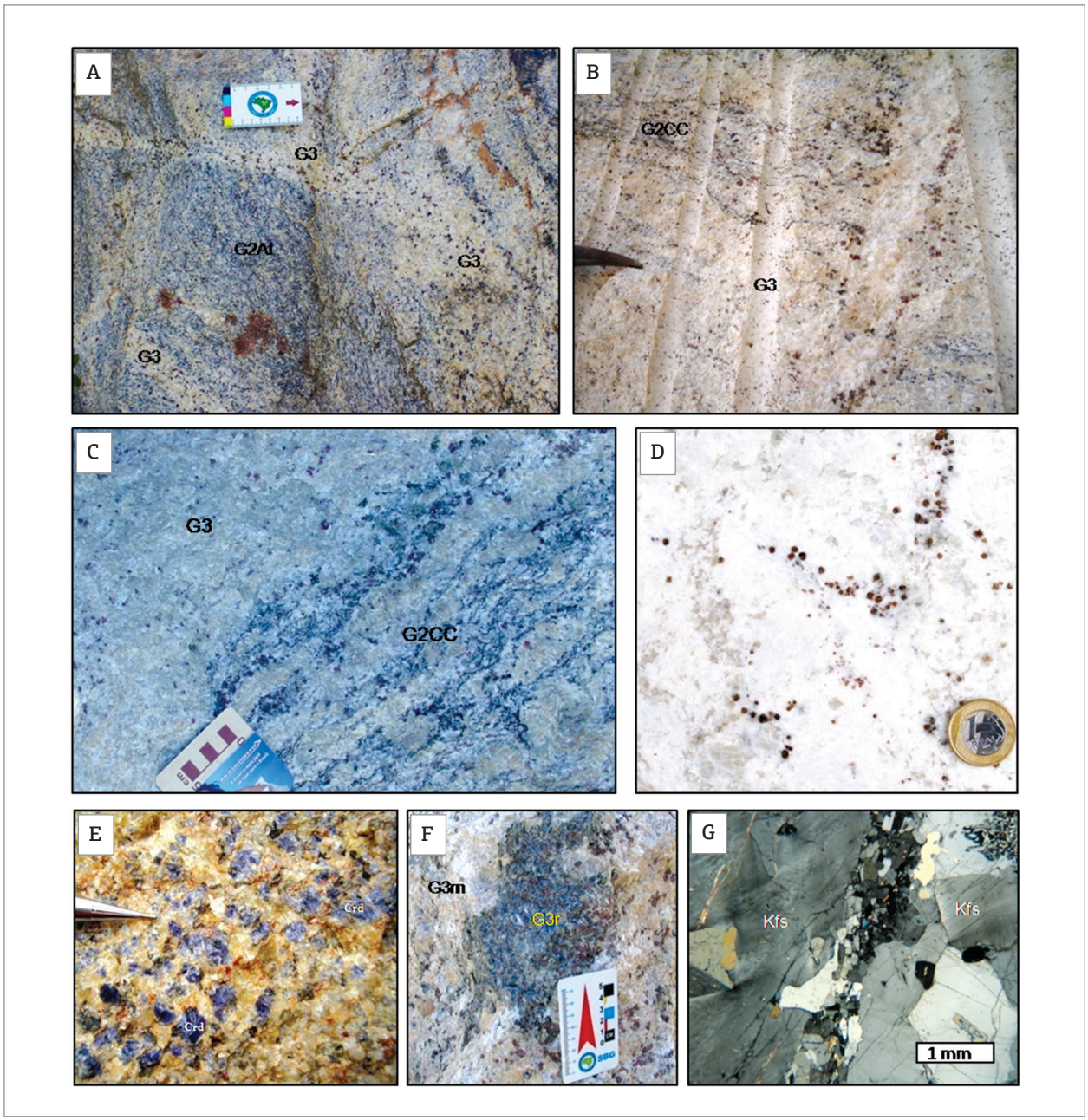

Figure 10. Photos from rocks of the G3 supersuite. (A) G3 leucosomes associated with Bt-rich Ataléia foliated granite (G2At); (B) G3 leucogranite with restites of Carlos Chagas foliated granite (G2CC); (C) contact between G3 leucogranite and Carlos Chagas foliated granite (G2CC); (D) G3 garnet leucogranite; (E) G3 cordierite leucogranite; (F) G3 leucogranite, representing the melt phase (G3m), associated with a rock composed of Crd+Grt+Sil+Ap (G3r), representing residuum from the partial melting process; (G) thin section (crossed polarizers) showing the Kfs-rich G3 leucogranite.

clastic rocks, relating clay-rich against quartz-rich sedimentary fractions; (ii) K_2O/Na_2O, concerning potassic components (mostly K-feldspar and biotite) versus plagioclase; and (iii) MgO/CaO, relating mafic components versus plagioclase (cf. Bhatia 1983, Taylor and McLennan 1985, Rosen 1992).

Paragneisses and cordierite granulites show SiO_2/Al_2O_3 ratios between clay-rich and quartz-rich sediments, suggesting a maturity index typical of graywackes (Fig. 11A). Most paragneisses have intermediate to high SiO_2/Al_2O_3 ratios, plotting in the graywacke to sub-graywacke/lithoarenite fields, with a small sample number representing graywacky pelite protoliths. Cordierite granulites tend to be richer in Al_2O_3 than paragneisses, suggesting that they derive from graywacky pelite protoliths (Fig. 11A). Both lithotypes outline similar

distributions in the MgO/CaO and K_2O/Na_2O fields, indicating quite balanced contributions of immature felsic to mafic components to their protoliths (Fig. 11A).

Taking into account that plagioclase is the main source of Ca and Na in carbonate-free clastic sediments, the lithochemical signature enriched in $CaO+Na_2O$ shown by most Nova Venécia samples suggests sources rich in intermediate to felsic rocks (such as calc-alkaline magmatic arcs, typical of active continental margin settings). Therefore, a plot of Na_2O/K_2O ratios versus silica (Fig. 11B) indicates that the Nova Venécia gneisses could be sediments formed within an active continental margin (Fig. 11).

From gneisses to granites

The Al-saturation diagram outlines the negative correlation trend of a series of peraluminous rocks, with Ataléia granites following down Nova Venécia gneisses, and clustering together with Carlos Chagas and G3 granites in the zone of low (A/NK)/(A/CNK) ratios (Fig. 12A). As expected from the petrographic studies, such trend agrees with the progressive depletion in biotite, as well as in other Al-rich mafic minerals, from the Nova Venécia paragneisses to the most evolved G2 and G3 granites.

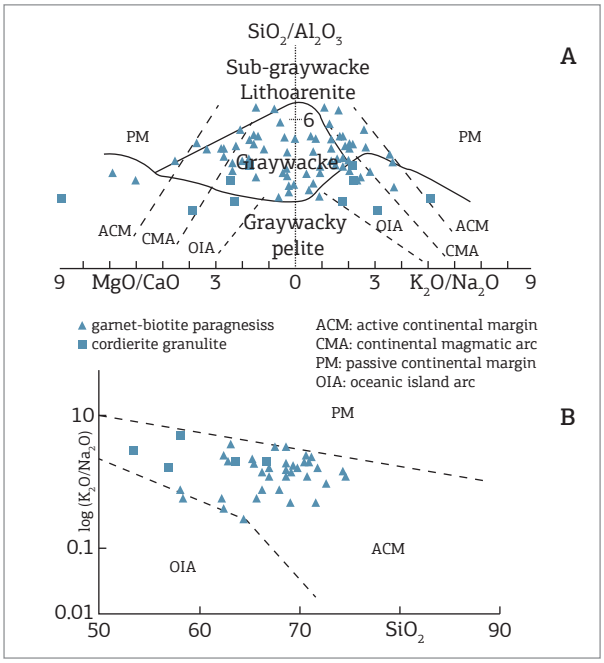

Figure 11. Plot of samples from the Nova Venécia Complex in diagrams suggested by (A) Rosen (1992), and (B) Bhatia (1983).

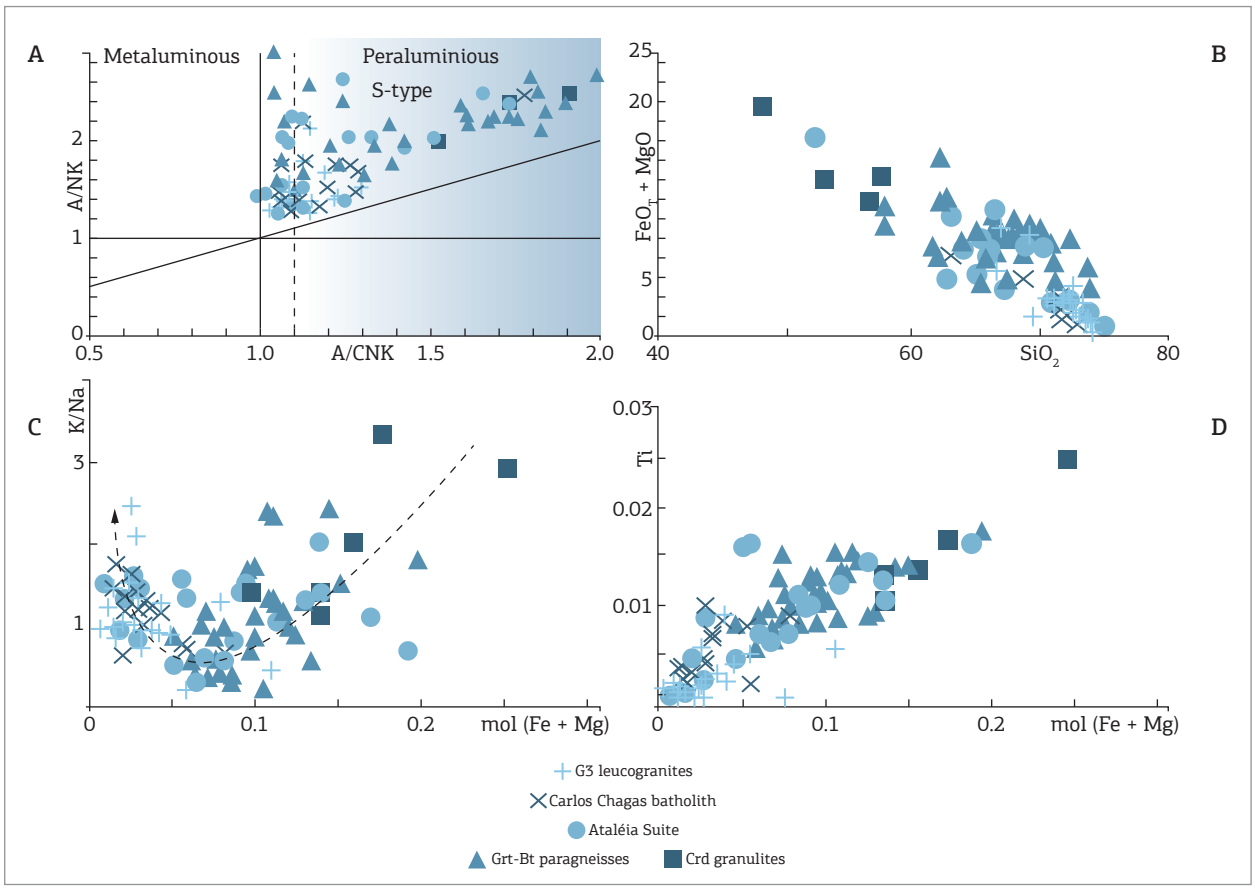

Figure 12. Lithochemical diagrams relating Nova Venécia gneisses, and G2 and G3 granites. (A) aluminum-saturation diagram; (B) silica versus total ferromagnesian (FeO_T+MgO) components; (C) maficity (mol (Fe+Mg)) versus alcalis ratio (K/Na); (D) maficity versus titanium (Ti).

The G2 and G3 granite samples plotting in the low-Al peraluminous zone (1.0 < A/CNK < 1.1; Fig. 12A) are not classical S-type granites (A/CNK > 1.1) neither I-type peraluminous granites (*cf.* Chapell & White 2001; Chapell *et al.* 2012). These low-Al peraluminous granites are the plagioclase-rich Ataléia granites, and some other G2 and G3 granites enriched in feldspars in relation to the Al-rich mafic minerals (Bt, Grt, Crd).

Lithochemical diagrams provide further evidence of the very close compositional relations between the Nova Venécia paragneisses and the Ataléia granites (Figs. 12 and 13), despite their obvious petrographic differences (Figs. 4 to 7). Indeed, the Ataléia granites closely overlap the Nova Venécia gneisses along almost the whole compositional trends (Fig. 12). This reflects the variable amounts of mafic minerals, as well as of residual plagioclase, inherited by the Ataléia melts from paragneisses. In fact, the Eu positive anomalies in Rare Earth Elements (REE) diagrams suggest plagioclase enrichment in samples from Ataléia granites, as well as in some Nova Venécia paragneisses (Figs. 13A and 13C). Moreover, mafic minerals from the Nova Venécia gneisses, such as garnet and ilmenite formed from the breakdown of biotite, would have been inherited by the Ataléia granites, probably according to the process of peritectic phase entrainment (Clemens & Stevens 2012). Nevertheless, the more differentiated Ataléia granites (i.e., richer in silica, Na and K, and more depleted in Ca and Mg+Fe) tend to plot apart from the Nova Venécia gneisses, but within the Carlos Chagas granite field (Fig. 12). REE patterns also indicate that many Ataléia granites represent less evolved melts in relation to Carlos Chagas granites (Figs. 13C and 13D). Bearing in mind that both the Ataléia and Carlos Chagas melts would be supplied by the same primary source (the Nova Venécia paragneisses), the compositional overlap zone discloses the chemical connection between the less evolved, autochthonous Ataléia melts and the more differentiated, semi-autochthonous to allochthonous Carlos Chagas melts.

Diagrams representing mafic components depict strong positive and negative correlations with Ti and Si, respectively, for the whole sample series (Figs. 12B and 12D). According to the petrographic information, these maficity correlation trends represent the progressive breakdown of biotite, together with the selective segregation between melting and residual phases, forming melts increasingly rich in silica and poor in mafic minerals. Such dehydrating anatectic process started in Al-rich gneisses and reached the Carlos Chagas and G3 granites, passing through most Ataléia granites that represent intermediate less-evolved G2 melts (Fig. 12). As expected, a clear tendency to K-enrichment appears from the Carlos Chagas to the G3 granites (Fig. 12C).

Although more scattered in the diagrams, data from the G3 leucogranites cluster close to the more differentiated G2 granites (Fig. 12). Mg# variations reflect their extreme differences in Grt/Crd modal ratios. In fact, the general lithochemical signature of G3 leucogranites agrees with the field and petrographic evidence, showing that they are partial melts from distinct varieties of G2 granites (Figs. 12 and 13). Some apparently anomalous REE patterns shown by G3 granites seem to be related to variations in the amounts of accessory minerals, such as apatite and monazite (Fig. 13).

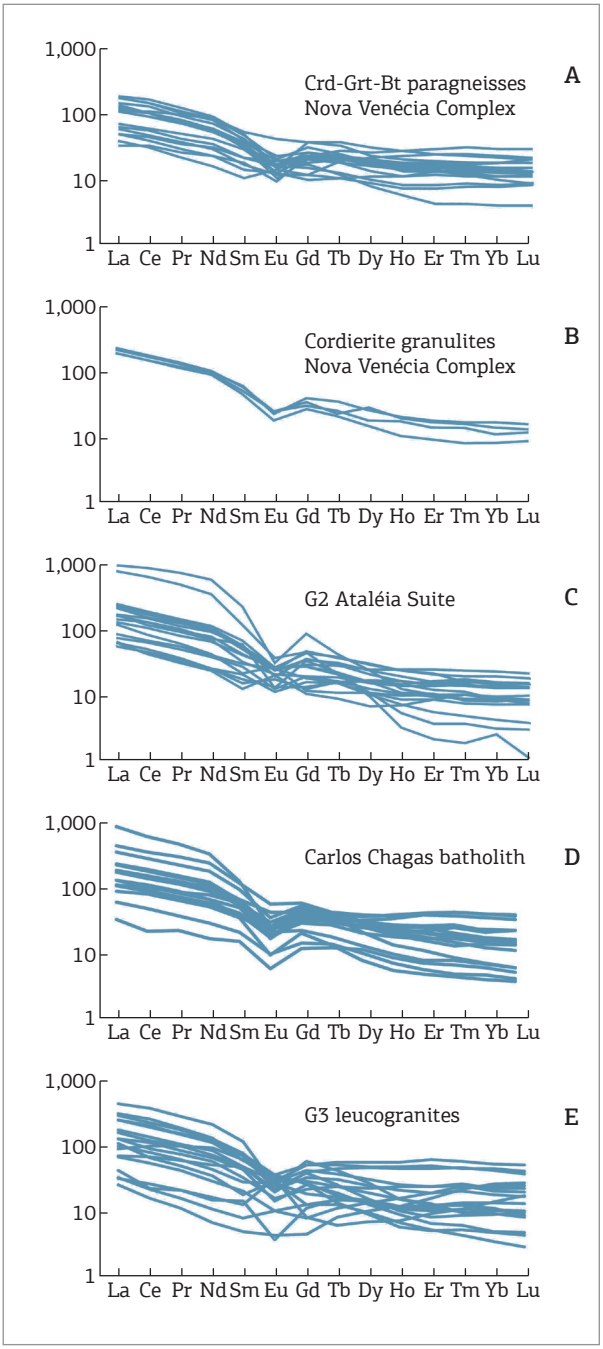

Figure 13. Chondrite normalized REE diagrams for samples of Nova Venécia paragneisses (A) and cordierite granulites (B), Ataléia granites (C), granites from the Carlos Chagas batholith (D), and G3 leucogranites (E). Normalizing factors are from Sun and McDonough (1989).

GEOCHRONOLOGY

We present here new geochronological results from isotopic U-Pb analysis in zircon, performed in the SHRIMP (Sensitive High Resolution Ion Microprobe) and LA-MC-ICP-MS (Multicollector Inductively-Coupled-Plasma Mass-Spectrometer) laboratory equipments of the Australian National University, the Universidade de Brasília and the Universidade Federal do Rio Grande do Sul. Sample preparation and analytical procedures, as well as the complete data tables are available in Gradim (2013).

Dating the eastern edge of the Rio Doce arc

Rocks of the Rio Doce arc occur along the western border of the study region, such as the northeastern tip of the Muniz Freire batholith in the surroundings of Afonso Cláudio, and the eastern massifs of the Baixo Guandu batholith (Fig. 2). These G1 rocks consist of migmatitic, foliated to banded tonalites, with stretched mafic to dioritic enclaves. U-Pb data for the Muniz Freire and Baixo Guandu batholiths suggest magma emplacement from ca. 625 Ma to ca. 585 Ma (De Campos *et al.* 2004; Pedrosa-Soares *et al.* 2011; Novo 2013).

Sample 479, from the Baixo Guandu batholith (Fig. 2), was selected for zircon U-Pb analysis, aiming to determine the age of the easternmost edge of the Rio Doce arc, and compare it with ages obtained for rocks of the back-arc zone. This sample was collected from a foliated Hbl-Bt tonalite with stretched mafic enclaves, free of anatectic leucosomes (Fig. 14). The selected crystals are clean prismatic zircons with oscillatory zoning and no significant overgrowth rims. From a few concordant spots on the cores of distinct zircon crystals (Fig. 14), the age of 589 ± 14 Ma was determined for the magmatic crystallization of the tonalite. This value agrees with the age (ca. 588 Ma) of the northeastern tip of the Muniz Freire batholith (Pedrosa-Soares *et al.* 2011), corresponding to the latest magma accretion along the easternmost border of the Rio Doce arc.

Detrital zircon data for the Nova Venécia Complex

Detrital zircon grains were selected from samples 11 and 484 of the Nova Venécia paragneisses (Fig. 2). Only the paleosomes were prepared for zircon concentration. The samples yielded a population of large (200-300 mm) detrital zircon grains, and only 17 reliable ages (Figs. 15A and 16).

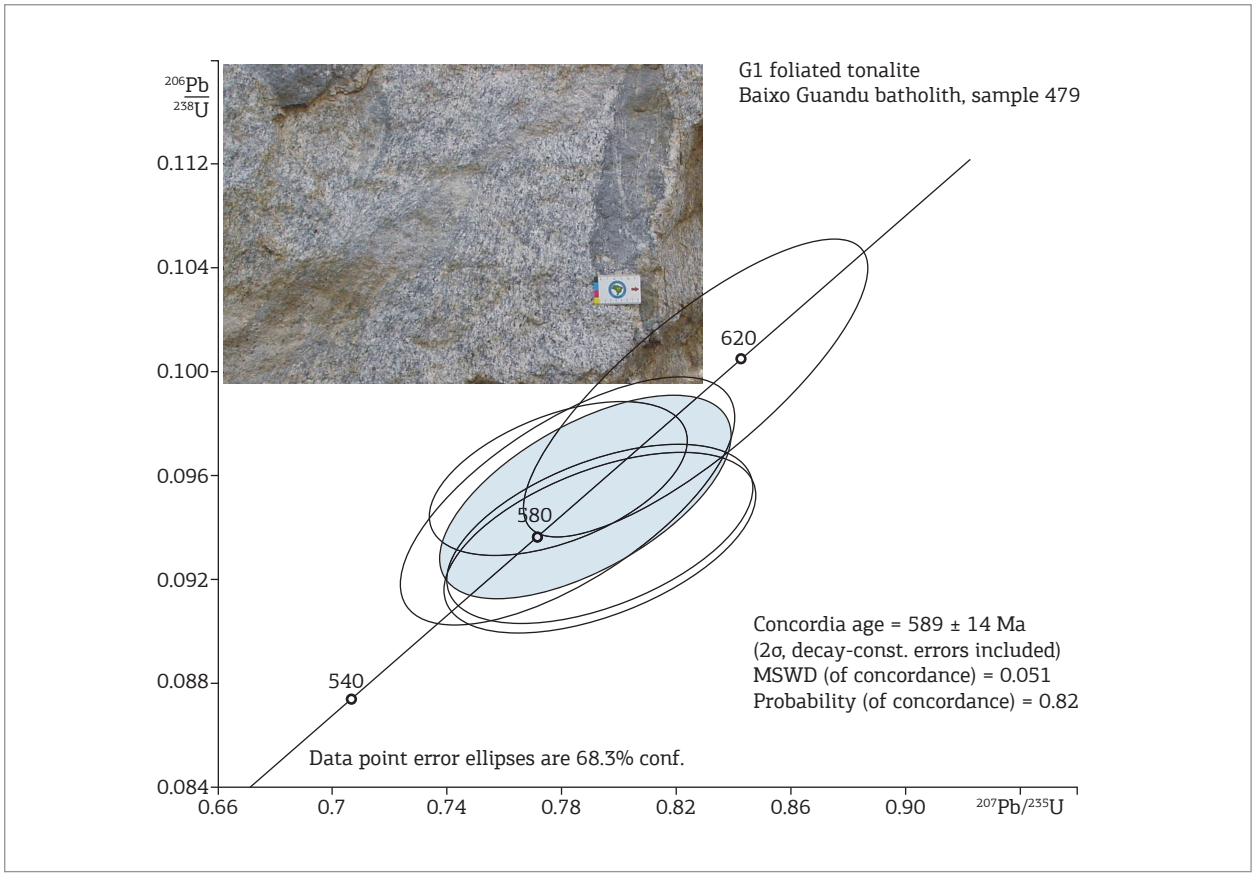

Figure 14. U-Pb concordia diagram for the Baixo Guandu foliated tonalite (sample 479, Fig. 2).

Figure 15. Selected zircon images (CL, cathodoluminiscence; EBS, electron backscattering). (A) detrital zircon grains from Nova Venécia paragneisses (sample 11, CL); (B) igneous and (C) metamorphic crystals from an Ataléia foliated granite (sample 66A, Fig. 17D, EBS); (D) igneous core and metamorphic rim in a zircon crystal from Carlos Chagas foliated granite (sample 66B, Fig. 17C), and (E) two metamorphic grains from 66B sample (EBS); (F) igneous crystals from a non-deformed isotropic Carlos Chagas granite (sample 21, CL); (G) metamorphic zircon grains from the ultramylonitic Carlos Chagas granite (sample 472); (H) zircon crystals from the Barra do São Francisco charnockite (sample 470, CL).

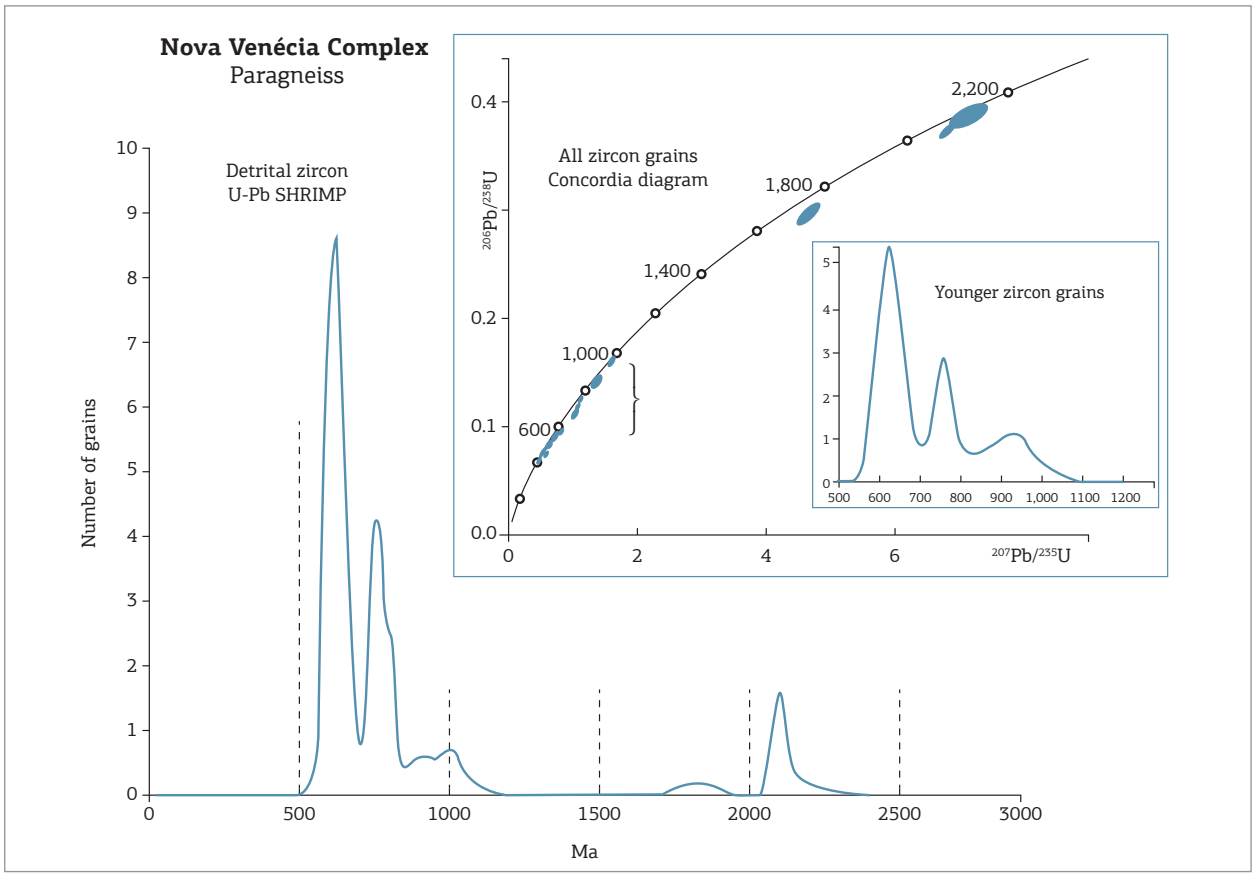

Figure 16. U-Pb age histogram for detrital zircon grains of the Nova Venécia paragneiss (samples 11 and 484, Fig. 2).

The grains display variety of internal structures which agree with the suggestion of multiple source areas for the sedimentary protolith. Most of them show oscillatory zoning and high Th/U ratios, typical of magmatic zircons (Fig. 15A).

Some general conclusions on time of deposition and sediment sources for the Nova Venécia basin can be established from the obtained ages. Four ages of sediment sources are indicated: (A) 590 – 641 Ma (44%); (B) 733 – 810 Ma (24%); (C) 2086 – 2124 Ma (11%); and (D) 901 Ma (only one grain). The first interval clearly indicates a significant sediment provenance from the nearby Rio Doce arc, including the Serra da Bolívia Complex (Noce *et al.* 2004; Pedrosa-Soares *et al.* 2011; Heilbron *et al.* 2013; Novo 2013). The second age interval B (733 – 810 Ma) suggests sedimentary contribution from the Rio Negro magmatic arc, located in the Ribeira belt (Tupinambá *et al.* 2012) or from the alkaline province of southern Bahia State (Rosa *et al.* 2007). The third age interval C records sediment provenance from the widespread Paleoproterozoic basement (Noce *et al.* 2007), and the isolated 901 Ma age grain may be derived from the Tonian rift-related magmatism of the precursor basin system (Pedrosa-Soares & Alkmim 2011).

The ages from the youngest zircon grains, around 600 Ma, point to a terminal Neoproterozoic basin fill coeval with the main development of the Rio Doce arc (Noce *et al.* 2004). The minimum sedimentation age might be constrained by the age of the metamorphic peak recorded in the Nova Venécia paragneisses, which has been dated around 575 Ma (Söllner *et al.* 2000; De Campos *et al.* 2004), as well as by G2 granite ages presented in the next section.

Dating G2 granites and regional metamorphism

We dated the non-deformed sample 21 of the Carlos Chagas granite, and the deformed and migmatized samples 66A and 475 of the Ataléia Suite, and samples 66B and 472 of the Carlos Chagas batholith. Within the outcrop 66 (Figs. 2 and 17), the Ataléia (66A) and Carlos Chagas (66B) foliated granites are in contact, and both enclose veinlets of the post-kinematic G3 leucogranite, represented by sample 66C (Fig. 17).

Images and Th/U ratios of zircon crystals from samples 66A (Ataléia foliated granite, Fig. 17D) and 66B (Carlos Chagas foliated granite, Fig. 17C) reveal both magmatic (Figs. 15B and 15D) and metamorphic (Figs. 15C and 15E)

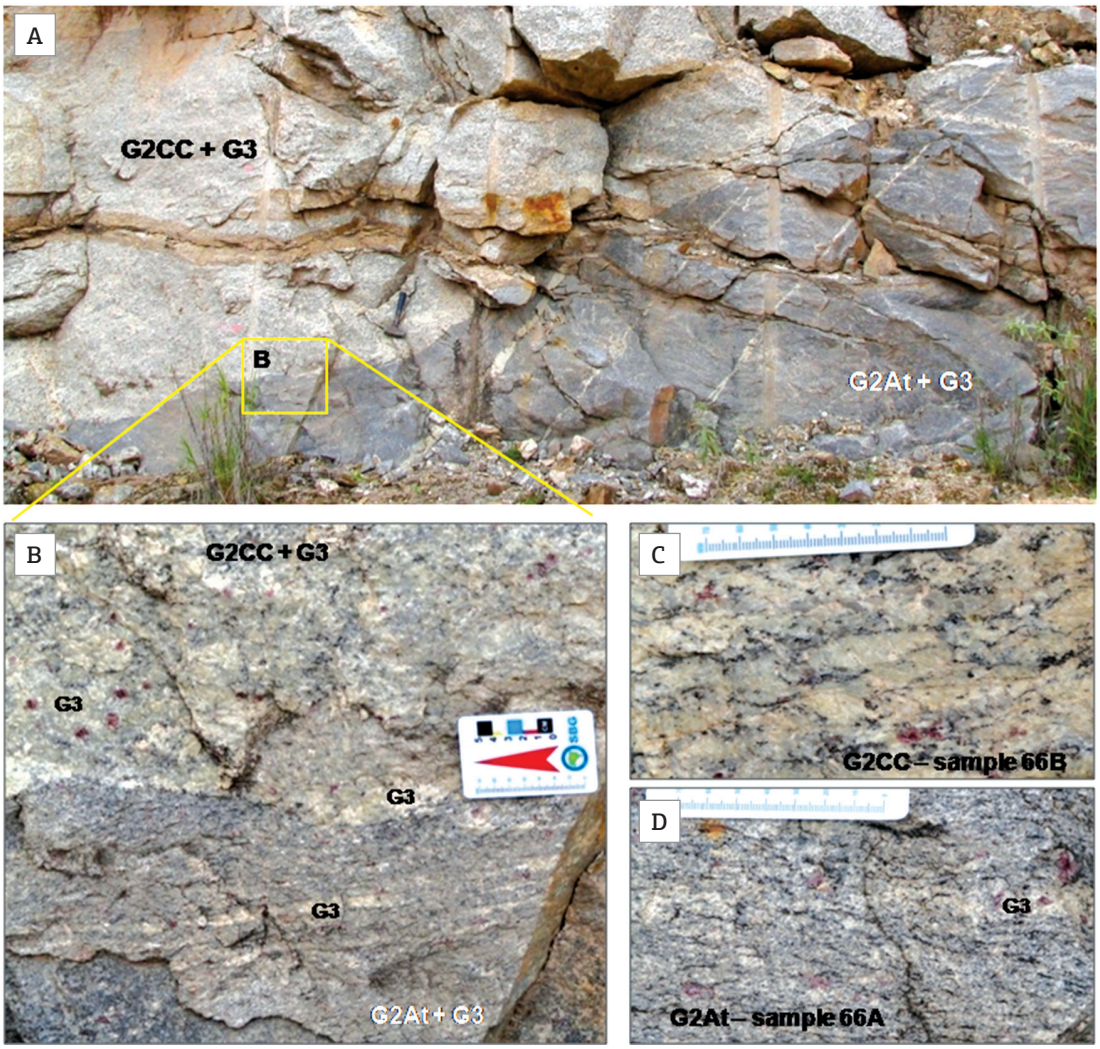

Figure 17. The outcrop 66 (A), showing the sharp contact between Ataléia and Carlos Chagas foliated granites (B–D), both enclosing small bodies of G3 leucogranite (B and D). Granitic veins cutting the Ataléia granite do not pass to the Carlos Chagas granite (A).

features. Zircon crystals from the non-deformed isotropic Carlos Chagas granite show typical magmatic features and Th/U ratios (Fig. 15F), whereas the highly deformed Carlos Chagas ultramylonitic granite is rich in zircon grains with metamorphic rims and very low Th/U ratios (Fig. 15G).

U-Pb data from zircon magmatic domains from the two samples (66A and 475) of the Ataléia foliated granites, collected in outcrops located some 100 km apart (Fig. 2), yielded the same crystallization age of about 588 Ma (Fig. 18A and B). Moreover, the Ataléia granite from the type locality, located ca. 50 km to the northeast of outcrop 66, yielded a zircon age of 591 ± 5 Ma (Noce *et al.* 2000). All together, these ages indicate the onset of the G2 granite generation around 590 Ma, in the back-arc zone.

In contrast, the U-Pb zircon ages from the Carlos Chagas granite suggest a much younger episode of granite emplacement in the back-arc zone. Zircon crystals from sample 21, an isotropic Carlos Chagas granite with no evidence of solid-state deformation (Fig. 8B), yielded a magmatic crystallization age at 576 ± 4 Ma (Fig. 18D), about 15 Ma later than the crystallization of the dated Ataléia granites. Additionally, we obtain the age of 568 ± 5 Ma for sample 66B of the Carlos Chagas foliated granite (Figs. 17C and 18E). These ages, together with similar data available in the literature (Silva *et al.* 2002, 2011; Vauchez *et al.* 2007), indicate the main period of magma emplacement in the Carlos Chagas batholith bracketed between 576 and 565 Ma.

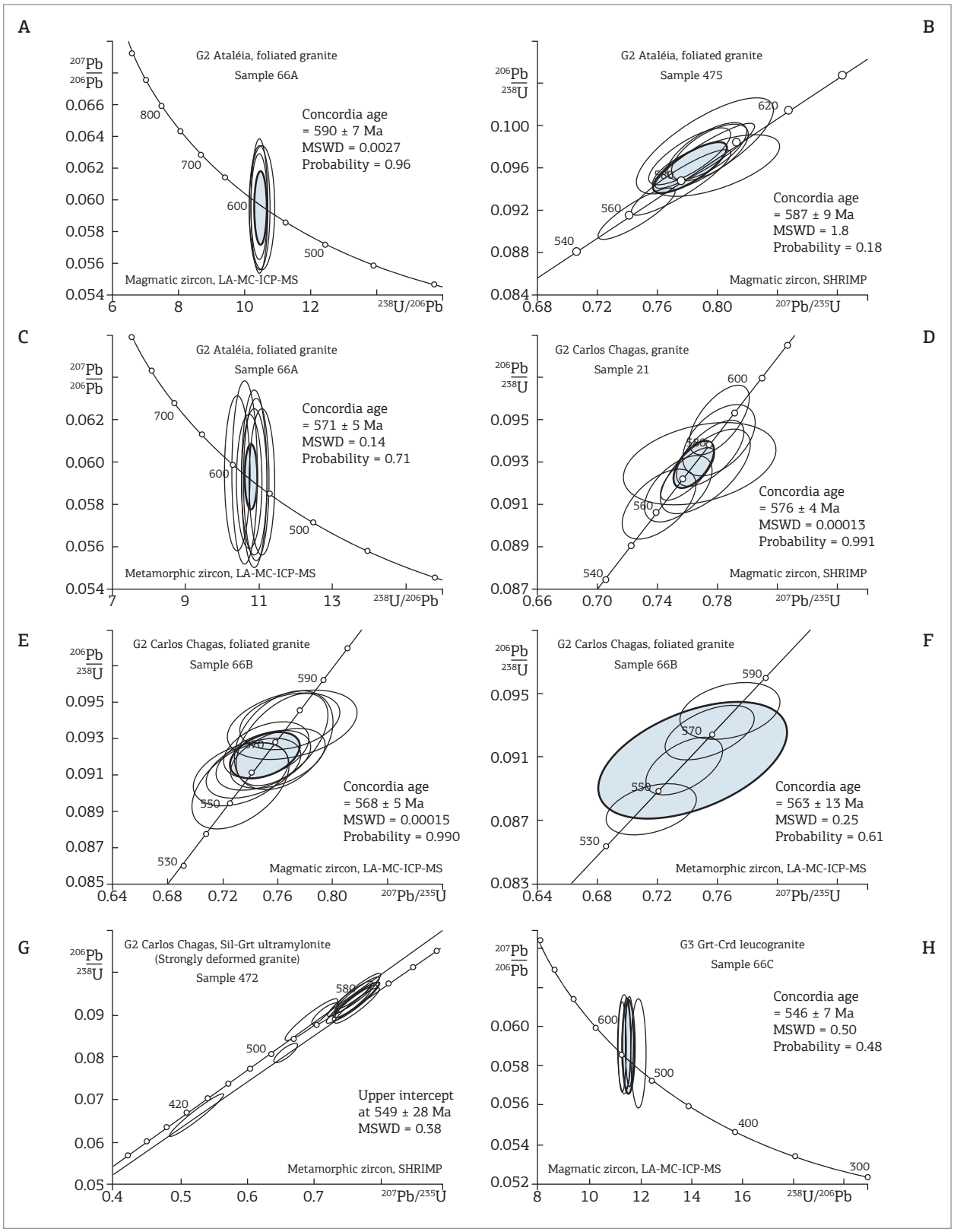

Figure 18. U-Pb concordia diagrams for samples from G2 and G3 supersuites. (A) sample 66A, Ataléia foliated granite (magmatic zircons); (B) sample 475, Ataléia foliated granite (magmatic zircons); (C) sample 66A, Ataléia foliated granite (metamorphic zircons); (D) sample 21, non-deformed Carlos Chagas granite; E, sample 66B, Carlos Chagas foliate granite (magmatic zircons); (F) sample 66B, Carlos Chagas foliated granite (metamorphic zircons); (G) sample 472, Carlos Chagas ultramylonitic granite (metamorphic zircos); (H) sample 66C, G3 leucogranite (magmatic zircons).

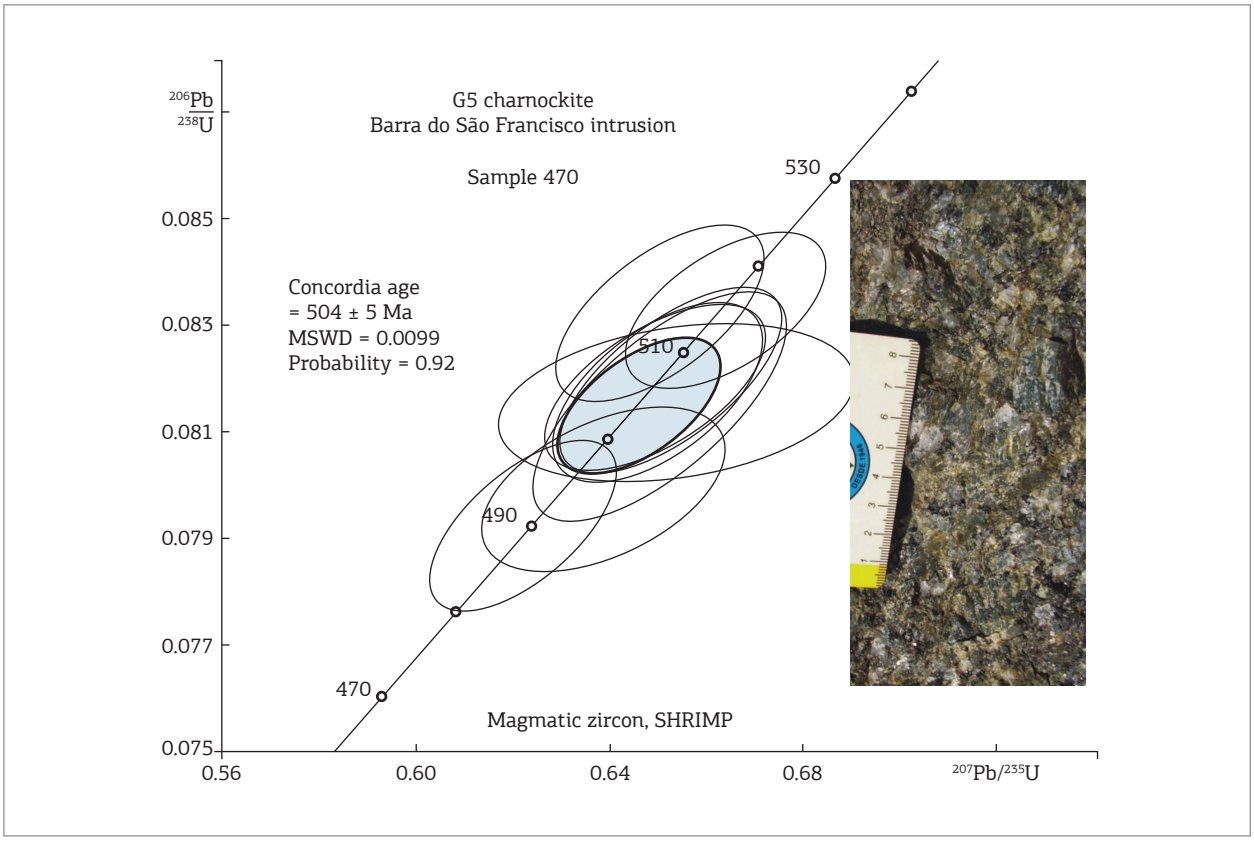

Figure 19. U-Pb concordia diagram for sample 470 (charnockite, G5 supersuite).

Metamorphic zircon data from samples 66A (Figs. 15C and 18C), 66B (Figs. 15E and 18F) and 472 (Figs. 15G and 18G) reveal ages related to the collisional tectono-metamorphic event. For example, the metamorphic recrystallization age of 571 ± 5 Ma for sample 66A (Fig. 18C) is ca. 20 Ma younger than the magmatic age from the same sample (590 ± 7 Ma, Fig. 18A). However, a similar age gap is not recorded by sample 66B, a Carlos Chagas foliated granite with stretched K-feldspar megacrists (Fig. 16C). In this sample, the magmatic crystallization is set at 568 ± 5 Ma (Fig. 18E), and metamorphic overprinting at 563 ± 13 Ma (Fig. 18F). These ages, similar within analytical error limits, suggest a syn-kinematic episode of magma emplacement, which was shortly followed by solid-state deformation in the Carlos Chagas batholith. Despite the age uncertainties due to the high-temperature mylonitization processes, the metamorphic zircon age of ca. 549 Ma given by the ultramylonitic granite 472 (Figs. 8K, 9F and 9G, 18G), could be related to a time limit for the final collisional processes for the Carlos Chagas batholith.

Dating a G3 leucogranite

Zircon crystals from sample 66C, a G3 leucosome found in outcrop 66, yielded a concordia age at 546 ± 7 Ma (Figs. 17 and 18H). This age, together with previous ages available in the literature (Silva *et al.* 2002; Noce *et al.* 2004; Pedrosa-Soares *et al.* 2011), constrain the G3 partial melting event from ca. 545 Ma to ca. 530 Ma, always in the back-arc zone.

Dating a G5 intrusion

The Barra do São Francisco intrusion mostly consists of charnockite, and minor Bt-Hbl granite (Gradim *et al.* 2005; Pedrosa-Soares *et al.* 2006a). The zircon U-Pb age of 504 ± 5 Ma of sample 470 constrains the magmatic crystallization of this G5 intrusion (Figs. 2, 15H and 19). This age is consistent with several age values recorded in the literature for G5 intrusions located in the back-arc zone (*e.g.*, De Campos *et al.* 2004; Mendes *et al.* 2005).

CONCLUSION

Back-arc basins related to active subduction zones and orogens develop over thin and hot lithospheric domains. Even when associated with continental magmatic arcs, back-arc domains can receive important heat inputs related to asthenosphere ascent and heat renewed by convection during the pre-collisional stage of the orogeny (Hyndman *et al.* 2005).

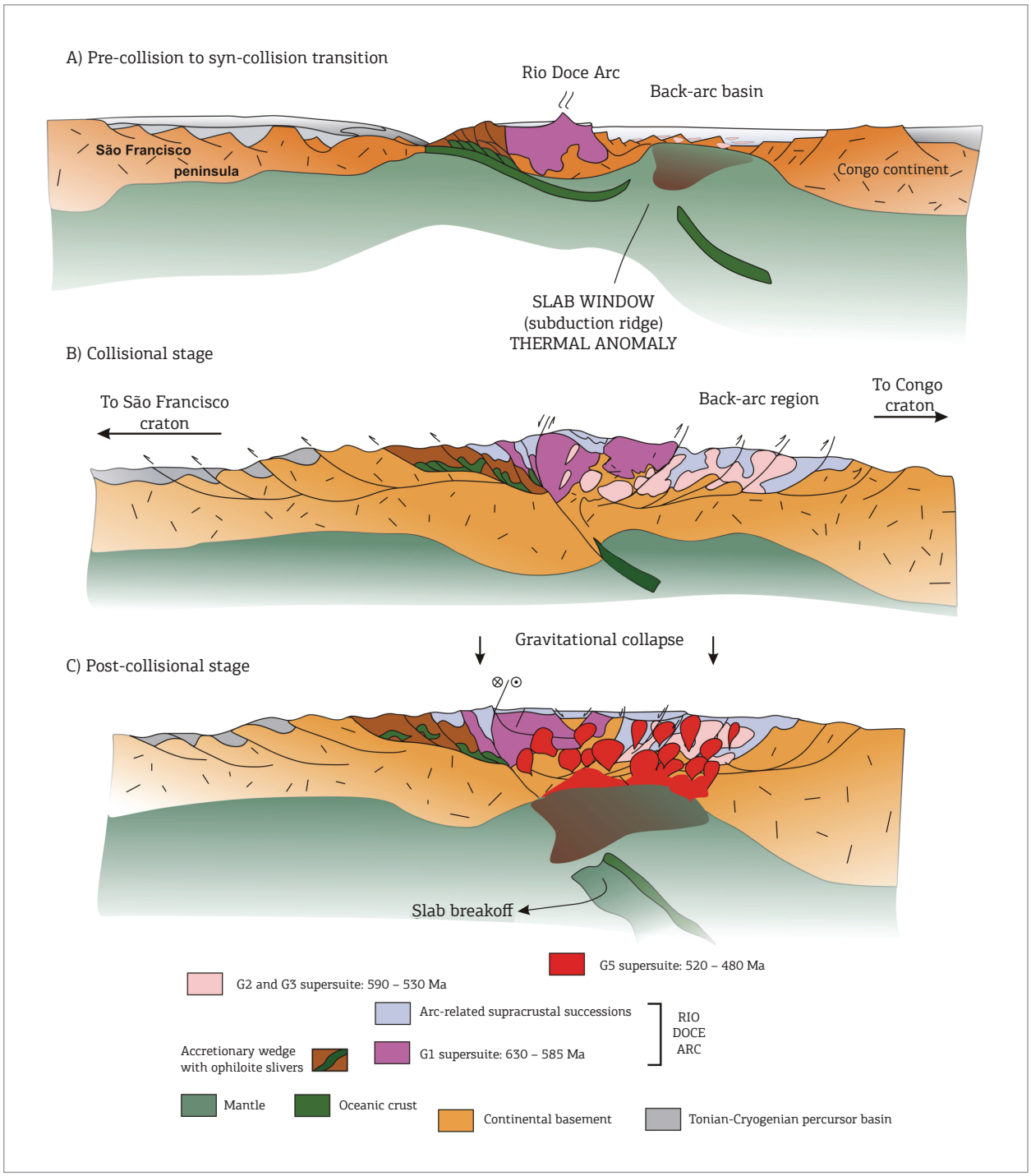

Figure 20. Paleotectonic cartoon illustrating the evolution of the back-arc region and granite generation events (A–C, not to scale).

The increase of heat supply in magmatic arcs may be caused by ridge subduction and associated slab window magmatism, together with slab breakoff and related gravitational collapse processes, producing significant to large amounts of granitic magmas in distinct stages of the orogenic evolution (De Long *et al.* 1979; Keskin 2003; Madsen *et al.* 2006).

The back-arc zone of the Araçuaí orogen records a long-lasting history (ca. 100 Ma) of granite generation events that produced a huge amount of collisional peraluminous granites, as well as post-collisional metaluminous intrusions. Our studies suggest that a series of peraluminous granitic melts (G2 Ataléia granites) started to form

by dehydration partial melting of metagraywackes (Nova Venécia paragneisses) in the back-arc zone, during the final pulses of development of the Rio Doce magmatic arc, around 590 – 580 Ma. This process may have been triggered by the subduction of a segment of the oceanic spreading center, with the onset of a thermal anomaly through a slab window under the back-arc basin, in the pre-collisional to syn-collisional transitional stage (Fig. 20A).

Following the first peraluminous melts, the dehydration anatectic process continuously proceeded and furnished melt to a huge accumulation zone of granitic magma, which crystallized slowly, giving birth to the collisional Carlos Chagas batholith, a gigantic granitic mass emplaced from ca. 580 Ma to ca. 560 Ma, with a climax around 575 Ma. This process was accompanied by a regional deformation and metamorphism related to the collisional stage. In our view, the heat supply for this event required combined processes, involving heat release from thrust stacking of the hot arc onto the back-arc, together with radiogenic heat release from the collisional thickened crust (Fig. 20B).

This huge amount of peraluminous granites underwent a late regional dehydration anatectic event, forming a much less voluminous leucogranite population, the G3 supersuite. Again, heat sources are required and, now, they may be related to the late heat release from the thickened granite-rich crust.

The onset of a new crustal heating of regional importance, the G5 plutonism, may have added further heat to the back-arc region of the orogen. This plutonism formed a myriad of intrusions generated during the climax of the gravitational collapse of the Araçuaí orogen, and the new heat supply would have been given by the asthenosphere ascent related to slab breakoff, followed by delamination of lithospheric mantle (Fig. 20C).

ACKNOWLEDGMENTS

The authors acknowledge financial support provided by Brazilian research and development agencies (CNPq, FAPEMIG and CODEMIG), the Geological Survey of Brazil (CPRM, Programa Geologia do Brasil), and the Brazilian oil company (PETROBRAS, Rede de Estudos Geotectônicos). The authors also owe their gratitude to Allen Nutman, Cristiane Castañeda, Daniel Gradim, Juliane Belém, Paulo Amorim Dias, Tiago Novo and Valter Vieira, for their contributions in analytical studies and mapping projects. Suggestions and reviews provided by Colombo Tassinari, Cristiano Lana, Marco Scambelluri, Omar Bartoli and anonymous reviewers greatly improved the original manuscript.

REFERENCES

Alkmim F.F., Marshak S., Pedrosa-Soares A.C., Peres G.G., Cruz S.C.P., Whittinton A. 2006. Kinematic evolution of the Araçuaí–West Congo orogen in and Africa: Nutcracker during the Neoproterozoic assembly of Gondwana. *Precambrian Research*, **149**:43-64.

Baltazar O.F. 2009. *Mapa geológico da Folha Linhares, 1:100.000*. Programa Geologia do Brasil, CPRM – Serviço Geológico do Brasil. Available from: www.geobank.sa.cprm.gov.br

Baltazar O.F. & Silva S.L. 2009. *Mapa geológico da Folha São Gabriel da Palha, 1:100.000*. Programa Geologia do Brasil, CPRM – Serviço Geológico do Brasil. Available from: www.geobank.sa.cprm.gov.br

Baltazar O.F., Zuchetti M., Oliveira S.A.M., Scandolara J., Silva L.C. 2010. *Folhas São Gabriel da Palha e Linhares*. Nota explicativa. Programa Geologia do Brasil, CPRM – Serviço Geológico do Brasil. Available from: www.geobank.sa.cprm.gov.br.

Bayer P., Horn H.A., Lammerer B., Schmidt-Thomé R., Weber-Diefenbach K., Wiedemann C. 1986. The Brasiliano Mobile Belt in Southern Espírito Santo (Brazil) and its igneous intrusions. *Zentralblatt f. Geologie und Paleontologie*. Teil I, **9/10**:1429-1439.

Belém J. 2006. *Caracterização mineralógica, física e termobarométrica deminérios de grafita da Província Grafítica Bahia–Minas*. MS Dissertation, Universidade Federal de Minas Gerais, Belo Horizonte, 165 p.

Bhatia M.R. 1983. Plate tectonics and geochemical compositions of sandstones. *Journal of Geology*, **91**:611-627.

Castañeda C., Pedrosa-Soares A.C., Belém J., Gradim D., Dias P.H.A., Medeiros S.R., Oliveira L. 2006. *Mapa Geológico e Nota Explicativa da Folha Ecoporanga, 1:100.000. In: Folha Ecoporanga*. Programa Geologia do Brasil, CPRM–UFMG (geobank.sa.cprm.gov.br), 50 p.

Chappell B.W. & White A.J.R. 2001. Two contrasting granite types: 25 years later. *Australian Journal of Earth Sciences*, **48**:489-499.

Chappell B.W., Colleen J.B., Doone W. 2012. Peraluminous I-type granites. *Lithos*, **153**:142-153.

Clemens J.D. & Stevens G. 2012. What controls chemical variations in granitic magmas? *Lithos*, **134-135**:317-329.

Cordani U.G. 1973. *Evolução Geotectônica da Região Costeira do Brasil, entre Salvador e Vitória*. Instituto de Geociências, Universidade de São Paulo, Tese de Livre Docência, 98 p.

Cordani U.G., Brito-Neves B.B., D'Agrella M.S., Trindade R.I.F. 2003. Tearing-up Rodinia: The Neoproterozoic paleogeography of South American cratonic fragments. *Terra Nova*, **15**:343-349.

Cordani U.G., Jacobsohn T., Sato K., Petronilho L., Ferreira T. 2005. On Samarium–Neodymium isochron dating of garnet and the role of inclusions. *Geophysical Research Abstracts*, **7**:05736.

De Campos C.M., Mendes J.C., Ludka I.P., Medeiros S.R., Moura J.C., Wallfass C. 2004. A review of the Brasiliano magmatism in southern Espírito Santo, Brazil, with emphasis on post-collisional magmatism. *Journal of the Virtual Explorer*, **17** (http://virtualexplorer.com.au/journal/ 2004/17/campos).

DeLong S.E., Schwarz W.M., Anderson R.N. 1979. Thermal effects of ridge subduction. *Earth and Planetary Science Letters*, **44**:239-246.

Féboli W.L. 1993a. *Programa Levantamentos Geológicos Básicos do Brasil. Domingos Martins. Folha SF 24–V–A–III. Estado do Espírito Santo*. Brasília. DNPM/CPRM. 180 p.

Féboli W.L. 1993b. *Programa de Levantamentos Geol. Básicos do Brasil. Piúma, Folha: SF.24–V–A–VI. Estado do Espírito Santo*. Brasília. DNPM/CPRM, 140 p.

Figueiredo M.C.H. & Campos-Neto M.C. 1993. Geochemistry of the Rio Doce Magmatic Arc, Southeastern Brazil. *Anais da Academia Brasileira de Ciências*, **65**:63-81.

Gonçalves-Dias T., Pedrosa-Soares A.C., Dussin I.A., Alkmim F.F., Caxito F.A., Silva L.C., Noce C.M 2011. Maximum sedimentation age and provenance of the Jequitinhonha Complex in the type–area (Araçuaí orogen): First U-Pb (LA–ICP–MS) data from detrital zircon grains. *Geonomos*, **19**:121-130.

Gradim C.T. 2013. *Complexo Nova Venécia e magmatismo associado, Orógeno Araçuaí, Estado do Espírito Santo, MS Dissertation*, Universidade Federal de Minas Gerais, Belo Horizonte, 96 p.

Gradim C.T., Queiroga G.N., Roncato J.G., Novo T.A., Pedrosa-Soares A.C. 2005. *Mapa Geológico da Folha Mantena 1:100.000*. Programa Geologia do Brasil, CPRM–UFMG (geobank.sa.cprm.gov.br).

Haralyi N.L.E. & Hasui Y. 1982. The gravimetric information and the Archean-Proterozoic structural framework of eastern Brazil. *Revista Brasileira de Geociências*, **12**:160-166.

Heilbron M., Tupinambá M., Valeriano C., Armstrong R., Eirado-Silva L.G., Melo R.S., Simonetti A., Pedrosa-Soares A.C., Machado N. 2013. The Serra da Bolívia complex: The record of a new Neoproterozoic arc-related unit at Ribeira belt. *Precambrian Research*, **238**:158-175.

Hyndman R.D., Currie C.A., Mazzotti S.P. 2005. Subduction zone backarcs, mobile belts, and orogenic heat. *Geological Society of America Today*, **15(2)**:4-10.

Keskin M. 2003. Magma generation by slab steepening and breakoff beneath a subduction–accretion complex: An alternative model for collision–related volcanism in Eastern Anatolia, Turkey. *Geophysical Research Letter*, **30**(24): doi:10.1029/2003GL018019.

Machado-Filho L. 1998. *Granulitos Azuis do Estado do Espírito Santo, geolojia e uso como rocha ornamental*. MS Dissertation, Universidade Federal do Rio de Janeiro, Rio de Janeiro, 85 p.

Madsen J.K, Thorkelson D.J., Friedman R.M., Marshall D.D. 2006. Cenozoic to Recent plate configurations in the Pacific Basin: Ridge subduction and slab window magmatism in western North America. *Geosphere*, **2**:11-34.

Mendes J.C., Medeiros S.R., McReath I., De Campos C. 2005. Cambro–Ordovician magmatism in SE Brazil: U-Pb and Rb–Sr ages, combined with Sr–Nd isotopic data of charnockitic rocks from the Várzea Alegre Complex. *Gondwana Research*, **8**:1-9.

Munhá J.M.U., Cordani U.G., Tassinari C.C.G., Palácios T. 2005. Petrologia e termocronologia de gnaisses migmatíticos da Faixa de Dobramentos Araçuaí (Espírito Santo, Brasil). *Revista Brasileira de Geociências*, **35**:123-124.

Nalini H.A., Bilal E., Paquette J. L., Pin C., Machado R. 2000a. Geochronologie U-Pb et géochimie isotopique Sr–Nd des granitoides neoproterozoiques des suites Galiléia et Urucum, Vallée du Rio Doce, Sud–Est du Brésil. *Comptes Rendus de l'Academie de Sciences Paris*, **331**:459-466.

Nalini H.A., Bilal E., Correia-Neves J.M. 2000b. Syncollisional peraluminous magmatism in the Rio Doce region: mineralogy, geochemistry and isotopic data of the Urucum Suite (eastern Minas Gerais State, Brazil). *Revista Brasileira de Geociências*, **30**:120-125.

Noce C.M., Macambira M.J.B., Pedrosa-Soares A.C. 2000. Chronology of late Proterozoic–Cambrian granitic magmatism in the Araçuaí belt, eastern Brazil, based on dating by single zircon evaporation. *Revista Brasileira de Geociências*, **30**:25-29.

Noce C.M., Pedrosa-Soares A.C., Piuzana D., Armstrong R., Laux J.H., De Campos C.M., Medeiros S.R. 2004. Ages of sedimentation of the kinzigitic complex and of a late orogenic thermal episode of the Araçuaí Orogen, northern Espírito Santo State, Brazil: Zircon and monazite U-Pb SHRIMP and ID–TIMS data. *Revista Brasileira de Geociências*, **34**:587-592.

Noce C.M., Pedrosa-Soares A.C., Silva L.C., Armstrong R., Piuzana D. 2007. Evolution of polyciclic basement complexes in the Araçuaí orogen, based on U-Pb SHRIMP data: Implications for Brazil–Africa links in Paleoproterozoic time. *Precambrian Research*, **159**:60-78.

Novo T.A. 2013. *Caracterização do Complexo Pocrane, magmatismo básico mesoproterozóico e unidades neoproterozóicas do sistema Araçuaí–Ribeira, com ênfase em geocronologia U-Pb (SHRIMP e LA–ICP–MS)*. Universidade Federal de Minas Gerais, Belo Horizonte, 193 p.

Paes V., Raposo F., Pinto C.P., Oliveira F. 2010. *Projeto Jequitinhonha, Estados de Minas Gerais e Bahia: texto explicativo. Geologia e Recursos Minerais das Folhas Comercinho, Jequitinhonha, Almenara, Itaobim, Joaíma e Rio do Prado*. Programa Geologia do Brasil. Belo Horizonte, CPRM, 376 p.

Pedrosa-Soares A.C. & Wiedemann-Leonardos C.M. 2000. Evolution of the Araçuaí Belt and its connection to the Ribeira Belt, Eastern Brazil. *In*: U.G. Cordani, E.J. Milani, A.Thomaz-Filho, D.A. Campos (eds.), *Tectonic Evolution of South America*. Sociedade Brasileira de Geologia, São Paulo, p. 265-285.

Pedrosa-Soares A.C., Vidal P., Leonardos O.H., Brito-Neves B.B. 1998. Neoproterozoic oceanic remnants in eastern Brazil: Further evidence and refutation of an exclusively ensialic evolution for the Araçuaí–West Congo Orogen. *Geology*, **26**:519-522.

Pedrosa-Soares A.C., Noce C.M., Wiedemann C., Pinto C.P. 2001. The Araçuaí–West-Congo Orogen in Brazil: An overview of a confined orogen formed during Gondwanaland assembly. *Precambrian Research*, **10**:307-323.

Pedrosa-Soares A.C., Queiroga G.N., Gradim C.T., Roncato J.G., Novo T.A., Jacobsohn T., Silva K.L. 2006a. *Nota Explicativa da Folha Mantena, 1:100.000*. Programa Geologia do Brasil, CPRM–UFMG (geobank.sa.cprm.gov.br).

Pedrosa-Soares A.C., Castañeda C., Queiroga G., Gradim C., Belém J., Roncato J., Novo T., Dias P., Gradim D., Medeiros S., Jacobhson T., Babinski M., Vieira V. 2006b. Magmatismo e Tectônica do Orógeno Araçuaí no Extremo Leste de Minas Gerais e Norte do Espírito Santo. *Geonomos*, **14**:97-111.

Pedrosa-Soares A.C., Alkmim F.F., Tack L., Noce C.M., Babinski M., Silva L.C., Martins-Neto M.A. 2008. Similarities and differences between the Brazilian and African counterparts of the Neoproterozoic Araçuaí–West-Congo orogen. *Geological Society, London, Special Publications*, **294**:153-172.

Pedrosa-Soares A.C. & Alkmim F.F. 2011. How many rifting events preceded the development of the Araçuaí–West Congo orogen? *Geonomos*, **19**:244-251.

Pedrosa-Soares A.C., De Campos C.P., Noce C., Silva L.C., Novo T., Roncato R., Medeiros S., Castañeda C., Queiroga G., Dantas E., Dussin I., Alkmim F. 2011. Late Neoproterozoic–Cambrian granitic magmatism in the Araçuaí orogen (Brazil), the Eastern Brazilian Pegmatite Province and related mineral resources. *Geological Society, London, Special Publications*, **350**:25-51.

Peixoto E., Pedrosa-Soares A.C., Alkmim F.F., Dussin I.A. 2013. A suture–related accretionary wedge formed in the Neoproterozoic Araçuaí orogen (SE Brazil) during Western Gondwanaland assembly. *Gondwana Research*, DOI: 10.1016/j.gr.2013.11.010.

Pinto C.P., Drumond J.B., Féboli W.L. (coords.) 2000. *Projeto Leste, Etapas 1 e 2*. CODEMIG, Belo Horizonte, 192 p., 26 mapas.

Queiroga G.N., Pedrosa-Soares A.C., Noce C.M., Alkmim F.F., Pimentel M.M., Dantas E., Martins M., Castañeda C., Suita M.T.F., Prichard F. 2007. Age of the Ribeirão da Folha ophiolite, Araçuaí Orogen: The U-Pb zircon dating of a plagiogranite. *Geonomos*, **15**:61-65.

Queiroga G.N., Pedrosa-Soares A.C., Roncato J.G, Dias P.H.A, Guimarães H.A., Coutinho M.O.G, Freitas N.C., Gradim C.T., Braga F.C.S., Novo T.A. 2012. *Mapa geológico e nota explicativa da Folha Nova Venécia, 1:100.000*. Programa Geologia do Brasil, CPRM–UFMG (geobank.sa.cprm.gov.br).

Richter F. 2013. *Unravelling crustal processes deep within the Araçuaí Orogen*. Universidade Federal de Ouro Preto, Ouro Preto, Trabalho de Conclusão de Curso, 47 p.

Roncato J.G. 2009. *As suítes graníticas tipo–S do norte do Espírito Santo na região das folhas Ecoporanga, Mantena, Montanha e Nova Venécia*, MS Dissertation, Universidade Federal de Minas Gerais, Belo Horizonte, 102 p.

Roncato J.G., Pedrosa-Soares A.C., Mascarenhas T.F., Fornero S.A., Galinari L.M., Gonçalves L.T., Queiroga G.N., Braga F.C.S, Novo T.A. 2012. *Geologia e recursos minerais da Folha Montanha SE.24–Y–B–I, Estados do Espírito Santo e Bahia, escala 1:100.000*. Programa Geologia do Brasil, Contrato CPRM–UFMG (geobank.sa.cprm.gov.br).

Rosa M., Conceição H., Macambira M., Galarza M.C., Cunha M., Menezes R., Marinho M., Cruz-Filho B., Rios D.C. 2007. Neoproterozoic anorogenic magmatism in the Southern Bahia Alkaline Province of NE Brazil: U-Pb and Pb–Pb ages of the blue sodalite syenites. *Lithos*, **97**:88-97.

Rosen O.M. 1992. Graywackes of the Precambrian metamorphic complexes: Composition and paleogeodynamic reconstructions. *International Geology Review*, **34**(12):1169-1186.

Signorelli N. 1993. *Programa Levantamentos Geológicos Básicos do Brasil. Afonso Cláudio. Folha SF 24–V–A–II. Estado do Espírito Santo*. Brasília. DNPM/CPRM. 153 p.

Siivola J. & Schmid R. 2007. *List of Mineral Abbreviations. IUGS Subcommission on the Systematics of Metamorphic Rocks*. Web version 01.02.07(www.bgs.ac.uk/scmr/home.html).

Silva J., Lima M., Veronese V., Ribeiro R., Siga Jr. O. 1987. Geologia. *In*: Projeto RADAMBRASIL. Folha SE 24 Rio Doce. IBGE, Rio de Janeiro (Levantamento de Recursos Naturais, 34).

Silva J.N. 1993. *Programa Levantamentos Geológicos Básicos do Brasil. Cachoeiro de Itapemirim. Folha SF–24–V–A–V. Estado do Espírito Santo*. Brasília. DNPM/CPRM, 165 p.

Silva L.C., Armstrong R, Noce C., Carneiro M., Pimentel M., Pedrosa-Soares A.C., Leite C., Vieira V.S., Silva M., Paes V., Cardoso-Filho J. 2002. Reavaliação da evolução geológica em terrenos pré-cambrianos brasileiros com base em novos dados U-Pb SHRIMP, parte II: Orógeno Araçuaí, Cinturão Móvel Mineiro e Cráton São Francisco Meridional. *Revista Brasileira de Geociências*, **32**:513-528.

Silva L.C., Pedrosa-Soares A.C., Armstrong R., Noce C.M. 2011. Determinando a duração do período colisional do Orógeno Araçuaí com base em geocronologia U-Pb de alta resolução em zircão: uma contribuição para a história da amalgamação do Gondwana Ocidental. *Geonomos*, **19**:180-197.

Sluitner Z. & Weber-Diefenbach K. 1989. Geochemistry of charnoenderbitic granulites and associated amphibolitic gneisses in the coastal region of Espirito Santo, Brazil. *Zentralblatt für Geologie und Palæontologie*, **1**(5/6): 917-931.

Söllner H.S., Lammerer B., Wiedemann-Leonardos C. 2000. Dating the Araçuaí–Ribeira mobile belt of Brazil. *Sonderheft, Zeitschrift Angewandte Geologie*, SH **1**:245-255.

Sun S.S. & McDonough W.F. 1989. Chemical and isotopic systematic of oceanic basalts: Implications for mantle composition and processes. *In*: A.D.Saumders and M.J.Morry (eds.), *Magmatism in Ocean Basins: Geological Society of London Special Publications*, **42**:313-345.

Taylor S.R. & McLennan S.M. 1985. *The Continental Crust:* Its Composition and Evolution. Blackwell, Oxford, 312 p.

Tuller M.P. 1993. *Programa Levantamentos Geológicos Básicos do Brasil. Colatina. Folha SF 24–Y–C–VI. Estado do Espírito Santo*. Brasília. DNPM/CPRM. 163 p.

Tupinambá M., Heilbron M., Valeriano C., Porto R., de Dios F., Machado N., Silva L.G., Almeida J. 2012. Juvenile contribution of the Neoproterozoic Rio Negro Magmatic Arc (Ribeira Belt, Brazil): Implications for Western Gondwana amalgamation. *Gondwana Research*, DOI: 10.1016/j.gr.2011.05.012.

Vauchez A., Egydio-Silva M., Babinski M., Tommasi A., Uhlein A., Liu D. 2007. Deformation of a pervasively molten middle crust: Insights from the Neoproterozoic Ribeira-Araçuaí orogen (SE Brazil). *Terra Nova*, **19**:278-286.

Vieira V.S. 1993. *Programa Levantamentos Geológicos Básicos do Brasil. Baixo Guandu. Folha SE 24-Y-C-V*. Brasília. DNPM/CPRM. 175 p.

Vieira V.S. 2007. *Significado do Grupo Rio Doce no contexto do Orógeno Araçuaí*, PhD Thesis, Universidade Federal de Minas Gerais, Belo Horizonte. 129 p.

Wiedemann C.M., Medeiros S.R., Mendes J.C., Ludka I.P., Moura J.C. 2002. Architecture of late orogenic plutons in the Araçuaí-Ribeira folded belt, Southeast Brazil. *Gondwana Research*, **19**:381-399.

Arquivo digital disponível on-line no site www.sbgeo.org.br